Response to reviewers for the paper "HO_x and NO_x production in oxidation flow reactors via photolysis of isopropyl nitrite, isopropyl nitrite-d_7, and 1,3-propyl dinitrite at λ = 254, 350, and 369 nm."

We thank the reviewers for their comments on our paper. To guide the review process we have copied the reviewer comments in black text. Our responses are in regular blue font. We have responded to all the referee comments and made alterations to our paper (**in bold text**).

Anonymous Referee #1

The author developed a new method using alkyl nitrite photolysis as a source of OH radical and NOx. Kinetic modeling was done to support that a much wider range of NO:HO2 ratio (10 -10000) was achieved. They present experimental and model characterization of the OH exposure and NOx levels generated via photolysis of C3 alkyl nitrites in the Potential Aerosol Mass (PAM) OFR. Together with chemical ionization mass spectrometer measurements of multifunctional oxidation, the author compared the products α-pinene generated following the exposure of to HOx and NOx obtained using both isopropyl nitrite and O3 + H2O + N2O methods. This new method proposed by Lambe et al. would open the prospect of OFR experiments at high NO. The paper is well written and organized. Few issues need to be addressed.

R1.1) While the author uses alkyl nitrates as a source of HOx and NOx in the oxidation flow reactor, their method provides a wider range of NO:HO2 ratio and lower OH exposure. The chemical ionization mass spectrometer measurements of α-pinene oxidation products from different alkyl nitrates experiments are somehow comparable to some ambient measurement. While this method sounds promising, I would also be glad to know any disadvantage of using this method as it is important for the oxidation flow reactor users to avoid unwanted chemical reactions. For example, by photolysis of alkyl nitrate, we will generate a lot of RO, RO2 and R radicals. These radicals may also involve in the further reactions with intermediates from the oxidation of injected VOCs. Therefore produce additional products other than only from the oxidation of injected VOCs. I wonder if the author observes any such kind of products in their mass spectra data? Is this process significant?

We modified the text as follows:

P12, L18-26: "Taken together, OFR254/**OFR**185-iN_2O and OFR369-i(iPrONO/iPrONO-d_7) are complementary methods that provide additional flexibility for NO_x-dependent OFR studies. **OFR254/OFR185-iN_2O generate variable-NO_x photooxidation conditions (NO:HO2≈0 - 100), and are suitable for the characterization of multigenerational oxidative aging processes at up to OH_{exp} ~ (5-10)*10^{11} molecules cm^{-3} s (~5-10 eq. days).** OFR369-i(iPrONO)/OFR369-i(iPrONO-d_7) generate high-NO photooxidation conditions ($NO:HO_2$≈10 - 10000) with minimal O_3 and NO_3 formation at longer photolysis wavelength than OFR254/185-iN_2O. We anticipate that alkyl nitrite photolysis is **advantageous** for the characterization of first-generation, high-NO_x photooxidation products of most precursors **at up**

to OH_{exp} ~ $1*10^{11}$ molecules cm^{-3} s (1 eq. day), which is comparable to environmental chambers investigating high-NO_x conditions. The generation of OD (rather than OH) via OFR369-i(iPrONO-d_7) may be useful in photooxidation studies of unsaturated precursors due to the shift on the m/z of the addition products, though at the potential expense of generating more complex distributions of oxidation products. **Potential disadvantages of using alkyl nitrite photolysis as a HO_x source are: (1) restriction to high-NO photochemical conditions; (2) restriction to OH_{exp} of 1 eq. day or less; (3) additional complexity involved with integration of the alkyl nitrite source (compared to O_3 + H_2O + N_2O); (4) potential inability to retrofit a specific OFR design with blacklights; (5) it acts as an interference that precludes NOx measurements by chemiluminescence detection.**

In regards to the reviewer's comment about R, RO, and RO2 radicals produced from isopropyl nitrite photolysis, the species that are treated in our model (R5-R17) include:

R: CH_3
RO: i-C_3H_7O, CH_3CO, HCO
RO2: CH_3O_2, $CH_3C(O)O_2$

Of the above species, in the presence of oxygen -- typically the case in most modern OFR studies -- all of the R and RO species (CH_3, i-C_3H_7O, CH_3CO, and HCO) are too short-lived to directly participate in reactions with RO_2 radicals formed from the oxidation of injected VOCs:

- CH_3 + O_2 generates CH_3O_2
- i-C_3H_7O + O_2 mostly generates HO_2 and acetone
- CH_3CO + O_2 generates $CH_3C(O)O_2$
- HCO + O_2 generates CO + HO_2

Thus, the most potentially problematic species include CH_3O_2 and $CH_3C(O)O_2$, which could participate in reactions with organic peroxy radicals generated from photooxidation of injected VOCs. Because generation of CH_3O_2 and $CH_3C(O)O_2$ only proceeds via iPrONO + hv → CH_3CHO + CH_3• + NO (R6), which has an estimated quantum yield of ~0.04 (P6, L16), the relative importance of these reactions is likely minor.

We modified the text as follows:

P6, L15-L16: "We assumed the quantum yield of Reaction R5 to be 0.5 **above 350 nm** (Raff and Finlayson-Pitts, 2010). **We assumed the quantum yield** of Reaction R6 to be 0.04 above 350 nm (value for t-butyl nitrite) (Calvert and Pitts, 1966), **suggesting minimal influence of CH_3O_2 and $CH_3C(O)O_2$ under these conditions that are generated via Reactions R7, R10, and R11 following iPrONO decomposition to CH_3 and CH_3CHO via Reaction R6. At 254 nm, the influence of CH_3O_2 and $CH_3C(O)O_2$ on ensuing photochemistry may be more significant. This is due to a higher quantum yield of Reaction R6 at 254 nm, which is estimated to be 0.86 under vacuum (Calvert and Pitts, 1966)."**

R1.2) P1 Line 4: Delete “t” before “λ = 254 nm”

Deleted.

R1.3) P3 Line 18-22: The author tried to use a NOx analyzer (Model 405 nm, 2B Technologies) to quantify the NO/NO2 mixing ratio. As shown in Figure S1 (b), the alkyl nitrates also show absorption at 405 nm which is the working wavelength of the NOx analyzer. Though the absorption cross section of alkyl nitrates is about one order of magnitude lower than that of the NO2, the mixing ratio of alkyl nitrates can be much higher than NO2, thus bias the NO2 and NO measurement. To perform the measurement, the author needs to correct the absorption by the alkyl nitrates.

Please see the text on P3, L23, where we stated that “we constrained [NO] and [NO_2] using the photochemical model discussed in Section 2.4” because we had difficulty correcting for absorption by the alkyl nitrites.

R1.4) P4 Line 20-24: To test this hypothesize, the author can simply measure the emission spectra of the UV lamps. This measurement can provide a direct proof to see the influence of longer wavelengths emission lines.

This is a fair point. We did not have access to an instrument that could measure the emission spectra of the 254 nm UV lamps; in the end, because OFR254-i(iPrONO) is not recommended, we did not pursue it further.

R1.5): A recent study by Ye et al. 2018 (ACP) found under wet conditions, heterogeneous uptake of SO2 onto organic aerosol was found to be the dominant sink of SO2, likely owing to reactions between SO2 and organic peroxides. This SO2 loss mechanism may bias the OH exposure measurement.

Thank you for the reference. In this work, OH exposure measurements were not conducted in the presence of organic aerosol (no VOCs were injected aside from alkyl nitrites, which themselves do not generate aerosol). Therefore we think that this is not an issue that is relevant to our results. However, we added the following sentence to the end of Section 2.2.2 to alert readers of the potential effect:

“While not applicable in this work, we note that heterogeneous uptake of SO_2 onto organic aerosol may bias OH exposure measurements (Ye et al., 2018).”

We added the following citation to references:

Ye, J., Abbatt, J. P. D., and Chan, A. W. H.: Novel pathway of SO_2 oxidation in the

atmosphere: reactions with monoterpene ozonolysis intermediates and secondary organic aerosol, Atmos. Chem. Phys., 18, 5549-5565, https://doi.org/10.5194/acp-18-5549-2018, 2018.

R1.6) P6 Line 23-24: I suggest the author add the reference data into that plot to show directly that their results are in good agreement with literature data.

We added isopropyl nitrite absorption cross sections obtained from λ = 300 to 450 nm by Raff and Finlayson-Pitts (2010) (black dashed line) to a revised Figure S1 shown below:

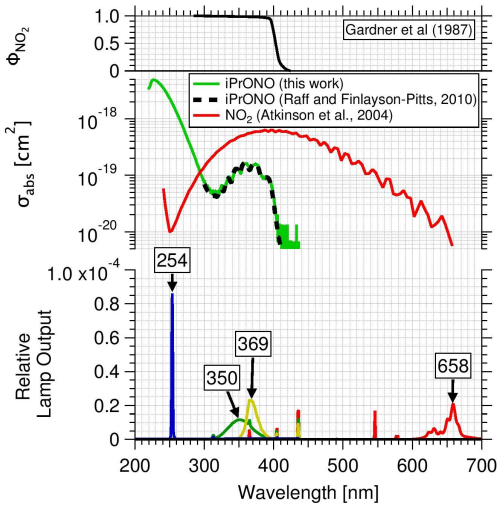

R1.7) P8 Line 6: Add "The model results showed that" before "For [iPrONO] ≤ 5 ppm".

We modified the text as follows:

P8, L6: "Figure 3 shows measured and modeled OH_{exp} and NOx concentrations obtained from photolysis of 0.5 to 20 ppm iPrONO [...] **The model results showed that for** [iPrONO] ≤5 ppm, OH_{exp} increased with increasing [iPrONO] because the rate of OH production increased faster than the rate of OH destruction from reaction with iPrONO and NO_2. For [iPrONO] > 5 ppm, the opposite was true and OH_{exp} plateaued or decreased. A maximum OH_{exp} =7.8×10^{10} molecules cm^{-3} s was achieved via photolysis of 10ppm iPrONO, with corresponding modeled [NO] and [NO_2] values of 148 and 405 ppb respectively."

R1.8) P11 Line 28-29: How much can NO3 radical be produced in the OFR? If this is already included in the model, the author could show the results to indicate how important of NO3 radical oxidation.

The maximum NO_3 concentration in the model cases in this study is only ~1 ppt, since there is no O_3 in OFR-i(iPrONO) and the second step of the $NO_2 \rightarrow HNO_3 \rightarrow NO_3$ oxidation chain by OH is slow. We thus do not report the negligible NO_3 concentrations in the figures but added the

following sentence at the end of Section 3.2:

"Modeled NO_3 concentrations were negligible in OFR-i(iPrONO) (<~1 ppt) because there is no O_3 present and NO_3 production via NO_2 + OH →HNO_3 and HNO_3 + OH →NO_3 + H_2O reactions was small."

Anonymous Referee #2

Summary and overall review: This manuscript evaluates the use of alkyl nitrite (AN) photolysis as an OH-precursor in an oxidation flow reactor (OFR). Experimental and model simulation approaches are used to constrain the parameters of interest to OFR studies such as the actinic flux calibration, amount of OH and NOx generation for different types of ANs as precursors. Empirical calibration equations are fit to observed data to create a domain of different OFR operational parameters such as residence time, external reactivity, etc. within which future AN-OFR experiments may operate. Finally, using chemical ionization mass spectrometry, it is shown that molecular structures of α-pinene SOA formed in the AN-OFR bear resemblance to that of ambient SOA previously observed in terpene-rich environments. The manuscript is topically relevant to AMT and builds on the body of literature regarding OFRs. However there are several shortcomings in the experimental description, outlined in my comments below, that must be addressed before it is ready for publication.

R2.1): The manuscript would benefit from a clearer description of the conditions when a PAM/OFR user would want to deploy nitrite as the OH precursor instead of using OFR185, OFR254, or injecting HONO. This manuscript demonstrates that AN can be used as a HOx precursor, but putting this method into better context with existing OFR practices would improve the manuscript.

Please see our response and updates to the paper text in response to a similar comment R.1.1 regarding comparison of OFR369-i(iPrONO) and OFR185/OFR254-iN2O. We anticipate that HONO will not be a useful HOx precursor in OFRs, as discussed in a new subsection below (please note that section has changed from Section 3.3.x to Section 3.5.x in response to comment 2.18):

3.5.2 Nitrous acid (HONO)

HONO is also commonly used as an OH radical source in environmental chamber studies. To evaluate its potential application in OFRs, we examined previous measurements in an environmental chamber equipped with blacklights, where photolysis of 3-20 ppm HONO generated initial [OH]~6×10^7 molecules cm^{-3} (Cox et al., 1980) which is 3.3 times lower than [OH] obtained from comparable levels of MeONO (Section 3.5.1). Lower OH_{exp} achieved from HONO photolysis is presumably due to higher OH reactivity of HONO relative to MeONO/iPrONO. Additionally, HONO is difficult to prepare without NO_2 impurities (Febo et al., 1995) that may cause additional OH suppression. For these reasons, we believe that there is no advantage to using HONO as a HO_x precursor in

OFRs.

We have added the following references:

A. Febo, C. Perrino, M. Gherardi, and R. Sparapani. Evaluation of a High-Purity and High-Stability Continuous Generation System for Nitrous Acid. Environmental Science & Technology 1995 *29* (9), 2390-2395.DOI: 10.1021/es00009a035.

Richard A. Cox, Richard G. Derwent, and Michael R. Williams. Atmospheric photooxidation reactions. Rates, reactivity, and mechanism for reaction of organic compounds with hydroxyl radicals Environmental Science & Technology 1980 *14* (1), 57-61. DOI: 10.1021/es60161a007

R2.2) OH estimation from SO2 and sulfate: (i) What collection efficiency was assumed for sulfate particles in the ACSM? (ii) An example of the sulfur mass balance should be shown (e.g., SO2 inlet, SO2 that survives the OFR, particulate SO4, SO2 lost to walls or other surfaces), at least in the SI.

(i) We assumed CE = 1, but for our purpose, the absolute CE value doesn't matter provided that the CE of sulfuric acid particles generated by SO_2 + OH via conventional OFR254 or via alkyl nitrite photolysis is the same. This assumption is justified based on the fact the humidity was similar for OFR254 and alkyl nitrite experiments and no ammonia (aside from presumably trace background levels) were present.

We modified the text as follows:

P4-5,L31-2: " To relate the measured [$SO_{2,0}$] and sulfate to OHexp, we conducted an offline calibration where 493 ppb SO2 was added to the reactor and OH was generated via O_3 + hv254 $\rightarrow O(^1D) + O_2$ followed by $O(^1D) + H_2O \rightarrow 2OH$ in the absence of NO_x. The reactor was operated at the same residence time **and humidity** used in alkyl nitrite experiments, **although we note that humidity will not change the response of the ACSM to sulfuric acid aerosols**. **Because no particulate ammonia was present aside from trace background levels, we assumed an ACSM collection efficiency of unity for the sulfate particles.**"

(ii) A sulfur mass balance is not possible because we could not unambiguously measure the SO_2 that survives the OFR due to apparent interferences in the SO_2 measurement (P4, L28). We added a new supplemental figure that illustrates this:

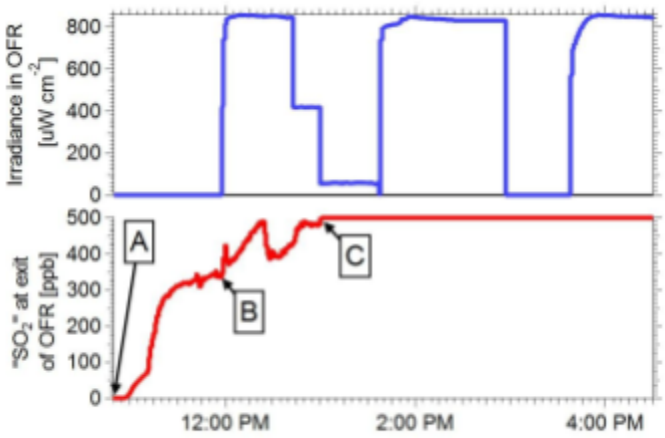

Figure S5. Example time series of SO_2 mixing ratio and irradiance (UV intensity) measured during a representative OFR369-i(iPrONO) OH_{exp} calibration. (A) Began SO_2 addition at OFR inlet with lamps off; 9.3 ppm iPrONO also added at OFR inlet (B) Lamps turned on after a steady-state SO_2 concentration of ~ 350 ppb was established (C) Analog output signal from SO_2 analyzer saturated due to apparent interference.

R2.3) OHexp estimation in Section 2.2.2: This work achieves < 1 day of OHexp and thus the uncertainties with estimating OHexp warrant more attention. One of the earlier OFR studies by Lambe et al. (2011) accounted for the influence of humidity on the growth of H2SO4 particles upon SO2 oxidation in the OFR. This section describes how calibration of OHexp v. particulate sulfate (from conventional OFR-254 method, hence in presence of humidity) was applied to measured particulate sulfate (from iPrONO photolysis, presumably also with humidity) to estimate OHexp.

R2.3a): It would be beneficial to briefly discuss how humidity was controlled in both these experiments and whether or not it was accounted for in correction of ACSM measured sulfate mass (unless sample was dried prior to ACSM sampling, in which case that should be specified).

We modified the text as follows:

P3, L11: "The relative humidity (RH) in the reactor was controlled in the range of 31-63% at 21-32°C **using a Nafion humidifier (Perma Pure LLC), with corresponding** H_2O volumetric mixing ratios of approximately 1.5-1.7%.

Please also see our response to R2.2, where we note that humidity does not affect the ACSM response to sulfuric acid aerosols.

R2.3b): It is not surprising that the sulfate mass responded linearly to increasing [SO2,0] in both these systems. The purpose of doing this inter-comparison was to see how much mass is formed in the iPrONO system v. in the conventional OFR-254 system, which would then imply how much OHexp is achieved in these two systems. Unless I am missing something, this comparison is not (but should be) plotted in Figure S5.

It was necessary to demonstrate a linear response between sulfate mass and [SO2,0] to illustrate that the sulfate particles were efficiently transmitted through the ACSM inlet aerodynamic lens (P5, L6-7). If they were not (e.g. too small or too large vs. the lens transmission window), we anticipate that the response would have been nonlinear.

We have revised Figure S4 (below; now Figure S6 in revised manuscript) to include the sulfate mass measured following SO_2 oxidation in the alkyl nitrite photolysis experiments compared with OFR254 experiments. The corresponding OH exposure for the alkyl nitrite systems was obtained by extrapolating the OFR254 calibration data to lower OH exposure.

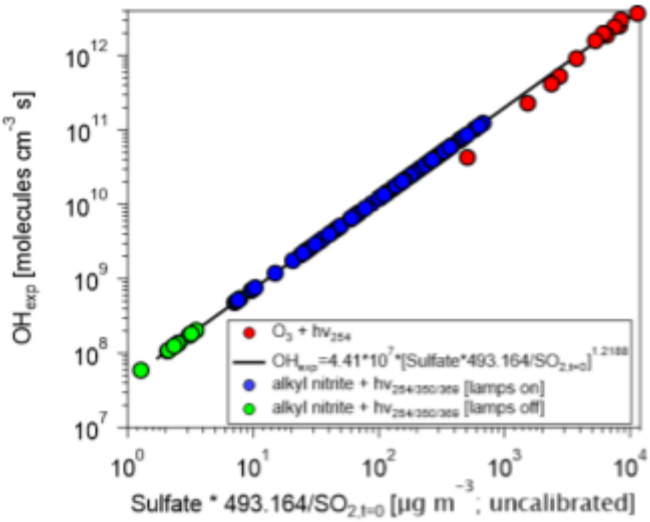

Figure S6. Calibrated OH_{exp} obtained following reaction of 493 ppb SO_2 with OH generated via $O_3 + h\nu_{254} \rightarrow O(^1D) + O_2$ followed by $O(^1D) + H_2O \rightarrow 2OH$ in the absence of NO_x **(red symbols)**. **The calibration equation was applied to measurements of sulfate formed during** alkyl nitrite **photolysis** experiments (**blue symbols**) **where SO_2 was added at the reactor inlet and the** reactor was operated at the same residence time. Particulate sulfate was measured with an Aerodyne Chemical Speciation Monitor. For details see Sect. 2.2

R2.4) Page 6, L18-19: How were the reductions in quantum yields for R6 and R5 determined? This seems like a critical assumption in the modeling and it is not explained in much detail. What is the sensitivity of the model predictions to these quantum yields?

We modified the text between L17-19 to clarify our rationales of this assumption. We also decide to change the upper limit quantum yield for Reaction R5 at 254 nm from 0.40 to 0.50 to reflect the value obtained by Raff and Finlayson-Pitts above 350 nm wavelength. The text now reads:

"At 254 nm, Calvert and Pitts (1966) estimated the quantum yield of Reaction R6 to be 0.86 under vacuum. **Assuming that all 254 nm photons initiate photolysis, the corresponding quantum yield of Reaction R5 is 0.14. Due to** collisional deactivation **at 1 atm** that prevent**s** i-C_3H_7O• decomposition**, the quantum yield of Reaction R5 at λ= 254 nm and 1 atm is expected to be higher than 0.14. Because quantum yield measurements were unavailable at these conditions, we applied an upper limit quantum yield of 0.50 as applicable at λ>350 nm and 1 atm (Raff and Finlayson-Pitts, 2010). We calculated a corresponding nominal quantum yield of 0.32 by averaging the lower and upper limit values of 0.14 and 0.50, resulting in a quantum yield of 0.68 for Reaction R6."**

Regarding the sensitivity of the model predictions to the quantum yield of Reaction R6, we modified text to Page 7, L29 to read:

"**Higher NO_2 concentrations were modeled at λ = 254 nm than at λ = 369 nm because more iPrONO was photolyzed and the NO_2 yield was only weakly dependent on the fate of i-C3H7O•. For example, NO is converted to NO2 either via reaction with HO2 obtained via Reaction R5 or CH3O2• and CH3C(O)O2• obtained via Reaction R6.** However, the effect of photolysis wavelength on **NO and** OH_{exp} was different. Specifically, the highest NO concentration and OH_{exp} was achieved via OFR369-i(iPrONO). OH_{exp} achieved via OFR369-i(iPrONO) was slightly higher than OH_{exp} attained using OFR350-i(iPrONO), likely because photolysis of both iPrONO and NO_2, whose reaction with OH suppresses OH_{exp}, is more efficient at λ = 369 nm than at λ = 350 nm (Figure S1 and Table 1). Further, the NO and OH yields achieved via OFR254-i(iPrONO) were suppressed due to significant (>**68**%) decomposition of i-C_3H_7O (Calvert and Pitts, 1966). The products of i-C_3H_7O decomposition, i.e., CH_3CHO and CH_3•, both have adverse effects with regard to our experimental goals: CH_3CHO is reactive toward OH and can thus suppress OH; the RO_2• formed through this reaction, $CH_3C(O)O_2$•, consumes NO **and generates NO_2** but does not generate OH; CH_3• rapidly converts to CH_3O_2•, which also consumes NO **and generates NO_2** but does not directly produce OH. **The dependence of OH, NO and NO_2 on the quantum yields of Reactions R5 and R6 was confirmed by sensitivity analysis of uncertainty propagation inputs and outputs as described in Section 2.4. OH_{exp} and NO were strongly anticorrelated with the quantum yield of Reaction R6, whereas the correlation between NO2 and the quantum yield of Reaction R6 was negligible."**

R2.5): The presentation of the equations in Page 10 needs to be improved. First, there seems to be a formatting issue – the first equation appears as equations 3-6 and the second as equations 7-9. Each equation should have one number. Second, I don't understand where these equations came from. Where are the data these equations are fit to (it should at least be shown in the SI)?

What is the quality of the fit? How was the functional form determined?

The equation formatting issue appears to be related to our attempt to implement multi-line equations using the Copernicus LaTeX template. We will follow up with the copy editing staff to resolve this issue.

To address the other questions from the reviewer, we modified text to Page 10, L11 to read:

"Fit coefficients were obtained by fitting Equations 3 and 6 to OH_{exp} model results over the following range of OFR parameters: ([iPrONO/iPrONO-d_7]; 0.2-20 ppm), I_{369} (1×10^{15} - 2×10^{16} photons cm^{-2} s^{-1}), OHR_{ext} (1-200 s^{-1}), and residence time, τ, between 30 and 200 sec. **We explored 11 logarithmically evenly distributed values in these ranges for each parameter, and thus performed simulations for 14641 model cases in total. To determine the functional form of Eqs. (3) and (6), we used the sum of the logarithms of first-, second-, and third-order terms of the four parameters and iteratively removed the terms with very small fit coefficients until further removal of remaining terms significantly worsened the fit quality."**

We also modified text on Page 10, L20 to read:

"Thus, we derived NO_2 estimation equations for OFR369-i(iPrONO) (Eq. 10) and OFR369-i(iPrONO-d_7) (Eq. 11) as a function of [RONO], I_{369}, and τ**, to all of which NO_2 is roughly proportional,** over the same phase space of model results used to **fit** Eqs. 3 and 6:"

The output data points of the model runs for fitting estimation equations (and the corresponding quantities estimated by the fitted equations) had already been shown in Fig. S7 of the AMTD version. The mean absolute values of the relative deviations of the equation estimates from the model outputs had already been reported to be 29% and 19% in Page 10, L14 and 26 for OH_{exp} and NO_2, respectively.

R2.6) Section 3.5: The comparison between the OFR and ambient CIMS spectra are presented only as in-line text. This comparison would be more effective if done graphically.

To Figure 5 (Figure 6 in the revised manuscript) we added panels (e) and (f) containing ambient NO_3^--CIMS spectra obtained from high-NO_x photochemical conditions in Centreville, Alabama, USA (Massoli et al., 2018) and in Hyytiala, Finland (Yan et al., 2016) We implemented an additional suggestion by this reviewer to add a separate panel (d) showing the -OD containing sticks (see R2.24).

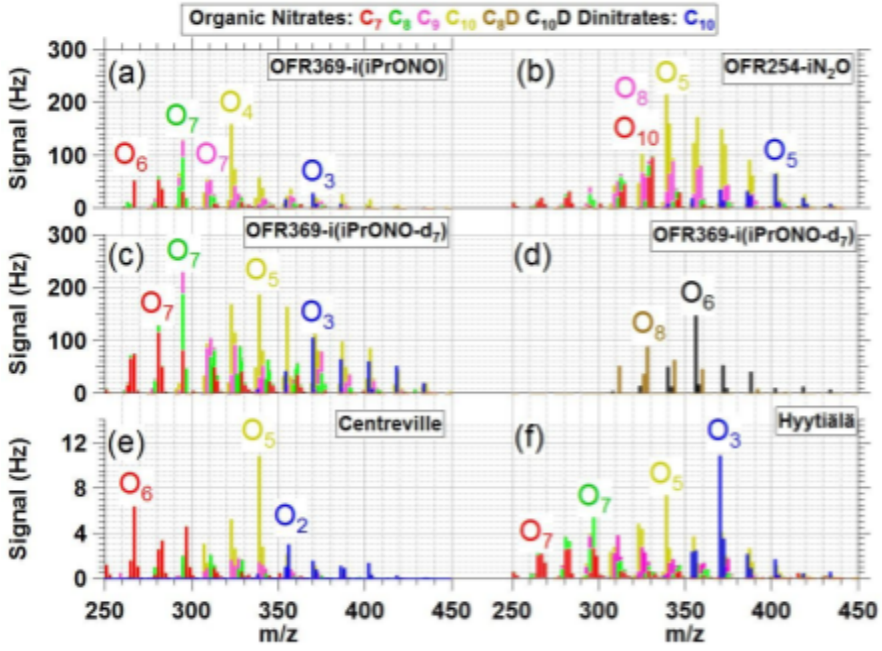

Figure 6. NO_3^--CIMS spectra of nitrogen-containing α-pinene photooxidation products with $C_{7-9}H_{9,11,13,15}NO_{5-10}$ ("C_7, C_8, C_9"), $C_{10}H_{15,17}NO_{4-14}$ ("C_{10}"), $C_8H_{8,10}DNO_{8-14}$ ("C_8D"), $C_{10}H_{14,16}DNO_{7-14}$ ("$C_{10}D$") or $C_{10}H_{16,18}N_2O_{6-13}$ ("C_{10} dinitrate") formulas generated via (a) OFR369-i(iPrONO) (b) OFR254-iN_2O (H_2O = 1%, N_2O = 3.2%). (c,**d**) OFR369-i(iPrONO-d7) **and observed in ambient measurements at (e) Centreville, Alabama, United States (Massoli et al., 2018) (f) Hyytiala, Finland (Yan et al., 2016).** "Ox" labels indicate number of oxygen atoms in corresponding signals (excluding 3 oxygen atoms per nitrate functional group).

We modified the text as follows:

"The ability of OFR369-i(iPrONO) and OFR369-i(iPrONO-d7) to mimic polluted atmospheric conditions can be evaluated by comparing signals observed in Figure **6** with published NO_3^--CIMS spectra obtained in Centreville, AL, USA (Massoli et al., 2018) and in Hyytiala, Finland (Yan et al., 2016). Both measurement locations are influenced by local biogenic emissions mixed with occasional anthropogenic outflow. **Figures 6e and 6f were obtained on 25 June 2013 (7:30–11:00 Centreville time) and 11 April 2012 (10:00-13:00 Hyytiala time) respectively. The mean NO mixing ratios during these periods were 0.53 ± 0.17 (Centreville) and 0.27 ± 0.09 ppb (Hyytiala).** In Centreville, the largest C10 nitrate and dinitrate species were **$C_{10}H_{15}NO_8$ and $C_{10}H_{16}N_2O_8$; in Hyytiala, $C_{10}H_{15}NO_8$ and $C_{10}H_{16}N_2O_9$ were the largest C10 nitrate/dinitrate signals. Elevated C_{10} dinitrate levels during the daytime in Hyytiaila (Figure 6f) suggests their formation from monoterpenes via two OH reactions followed by two RO_2 + NO termination reactions, as proposed earlier. Overall, Figure 6 shows that many of the C7-C10 nitrogen-containing compounds observed in Centreville and Hyytiala** were generated via OFR369-i(iPrONO), OFR369-i(iPrONO-d7) and

OFR254-iN_2O. **D**ue to the local nature of the ambient terpene emissions at the Centreville and Hyytiala sites, the associated photochemical age was presumably <1 day. Thus, while the ambient NO_3^--CIMS spectra at those sites were more complex and contained contributions from precursors other than α-pinene, the oxidation state of the ambient terpene-derived organic nitrates was more closely simulated via OFR369-i(iPrONO) or OFR369-i(iPrONO-d7), where the largest C10 nitrates and dinitrates were $C_{10}H_{15}NO_7$ and $C_{10}H_{16}N_2O_9$ (OFR369-i(iPrONO); Figure 5a), and $C_{10}H_{15}NO_8$, $C_{10}H_{15}NO_9$ and $C_{10}H_{16}N_2O_9$ (OFR369-i(iPrONOd7); Figure 5c). By comparison, $C_{10}H_{15}NO_8$ and $C_{10}H_{16}N_2O_{11}$ were the largest nitrate and dinitrate species generated via OFR254-iN2O (Figure 5b)."

R2.7) Relevance of this study for "Mimicking polluted atmospheric conditions": the manuscript addresses a key limitation of the N2O-OFR, in which, achieving < 1 equivalent day of NOx dependent SOA formation is challenging. While the use of ANs as OH (or OD) precursors is shown to be promising for achieving such low oxidative exposures in this study, this potentially makes OH suppression a major concern for in-situ deployment of the AN-OFR (Peng et al. 2015). The chemical composition of α-pinene SOA formed in the AN-OFR (this study) bears resemblance to SOA previously observed in terpene-rich conditions in Centerville, Alabama and Hyytiälä, Finland (Yan et al., 2016; Massoli et al., 2018), suggesting that OH suppression may not be an issue. However, the manuscript lacks description of how much α-pinene was injected into the OFR, whether OH suppression was a competing influence, and if yes, whether or not it was accounted for.

We modified the text as follows:

P11, L3: "To evaluate the efficacy of OFR369-i(iPrONO), OFR369-i(iPrONO-d_7), and OFR254-iN_2O [...] the reactor was operated with a residence time of approximately 80 sec to accommodate the undiluted NO_3^--CIMS inlet flow requirement (10.5 L min^{-1}). OFR369-i(iPrONO) and OFR369-i(iPrONO-d_7) were operated using I_{369} = 6.5×10^{15} photons cm^{-2} s^{-1}, >7 ppm nitrite, **and 500 ppb a-pinene**. OFR254-iN_2O was operated using I_{254} =3.2×10^{15} photons cm^{-2} s^{-1}, 5 ppm O_3 + 1% H_2O + 3.2% N_2O, **and 16 ppb α-pinene**. Corresponding **calculated** OH exposures were 2.9×10^{10}, 5.9×10^{10} and **5.0**×10^{11} molecules cm^{-3} s, respectively, **in the absence of OH consumption due to α-pinene. These calculated steady-state OH_{exp} values decreased to 8.5×10^8, 6.8×10^8 and 4.6×10^{11} molecules cm^{-3} s after accounting for OH consumption. This suggests that most of the OH that was produced in these OFR369-i(iPrONO/iPrONO-d_7) experiments was consumed by α-pinene and its early-generation photooxidation products. We note that OH suppression relative to 254 nm photons, O_3, and O is not a concern in OFR369-i(iPrONO), unlike OFR254-iN_2O (Peng et al., 2016)."**

R2.8) Abstract line 3: extra "t" before λ.

Deleted (see also reply to R1.3).

R2.9) Equation 1: I assume that density is for the liquid, but please specify.

We modified the text as follows:

P3, L5-6: "where [...] ρ (g cm^{-3}) and MW (g mol^{-1}) are the organic nitrite **liquid** density and molecular weight…"

R2.10) P1 L17: space needed before (Mao et al., 2009…). This error repeats several times in citations throughout the manuscript.

We fixed this error in the revised manuscript.

R2.11) P2 L13: in the presence of humidified air (if I am understanding the reactions correctly).

No - water vapor is not required for HO_x + NO_x generation via alkyl nitrite photolysis.

R2.12) Page 3, L14: the light manufacturer LCD Lighting is listed in this line but not the previous lines.

Yes, LCD Lighting is the light manufacturer. The part numbers listed in previous lines (F436T5/BL/4P-350, F436T5/BLC/4P-369) were formatted per the preference of LCD Lighting, Inc., where they manufactured the lamps as OEM equipment and then renamed the end products with part # and reference to Aerodyne Research.

R2.13) P3 L18-23: Is it possible to include some numbers describing this interference (maybe in the SI)? How was the conclusion of "no avail" drawn? Did the 2B monitor read increasing [NOx] with increasing [iPrONO] injection into dark OFR? Since this AN photolysis is a unique aspect of this manuscript, I think instrumental caveats should be better described.

Yes, exactly - the 2B monitor read increasing [NO_x] with increasing [iPrONO] injection into dark OFR (both NO and NO_2 channels).

We modified the text as follows:

P3, L18-23: "NO and NO_2 mixing ratios were measured using a NO_x analyzer (Model 405 nm, 2B Technologies), which quantified [NO_2] (ppb) from the measured absorbance at λ= 405 nm, and [NO] (ppb) by reaction with O_3 to convert to NO_2. Alkyl nitrites introduced to the reactor with the lamps turned off consistently generated signals in the both NO and NO_2 measurement channels of the NO_x analyzer, possibly due to impurities **and/or species generated via iPrONO + O_3 reactios inside the analyzer**. **For example, background NO and NO_2 mixing ratios increased from 0 to 1526 ppb and 0 to 1389 ppb as a function of injected [iPrONO] = 0 to 18.7 ppm** with the lamps off (**Figure S2**). We attempted to correct [NO] and [NO_2] for this apparent alkyl nitrite interference by subtracting background signals measured in the presence

of alkyl nitrite with lamps off, to no avail, **because background signals (alkyl nitrite present with lamps off) were large compared to signals obtained with alkyl nitrite present with lamps on**. Instead, we constrained [NO] and [NO_2] using the photochemical model discussed in Section 2.4."

We added a figure to the supplement (below):

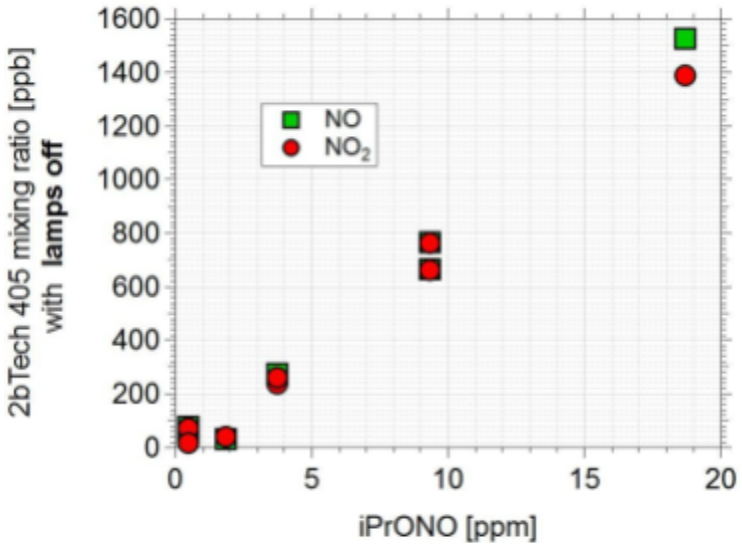

Figure S2. "NO" and "NO_2" mixing ratios measured at the exit of the reactor as a function of isopropyl nitrite added to the reactor inlet with the lamps off.

R2.14): Somewhere in the methods section, the authors should mention what was the flow through the OFR in the calibration experiments. The flow rate through OFR for CIMS experiments is mentioned later, but the flow rate in non-CIMS experiments is not mentioned anywhere.

We modified the text as follows:

P3, L11: "Alkyl nitrites were photolyzed inside a Potential Aerosol Mass (PAM) oxidation flow reactor [...] operated in continuous flow mode (Lambe et al., 2017) **with 5.1±0.3 L/min flow through the reactor unless stated otherwise.**"

R2.15) P8 L5: this sentence is confusing, because it suggests that measured values of NOx are shown in Figure 3, while in fact they are not. Should be reworded accordingly.

The original sentence read: "Figure 3 shows measured and modeled OH_{exp} and NO_x Concentrations". We reworded the sentence to state: "Figure 3 shows measured OH_{exp} and **modeled** NO_x concentrations."

R2.16) P8 L30 (and Figure 4): the explanation of higher NOx offsetting OH production efficiency seems straightforward enough that it should be reproduced by KinSim. However, it seems the model was not run (or not plotted in Figure 4) for this OFR369-i(1,3-Pr(ONO)2) scenario. Can this be explained?

Constraints on the OH rate constant and absorption cross section of 1,3-Pr(ONO)2 are required to model OFR369-i(1,3-Pr(ONO)2). In this case, literature values were not available and we did not feel we could adequately constrain the rate constant and cross section from first principles or structure-activity relationships.

R2.17): Again, the caption for Figure 4 is confusing because "measured and modeled values … of (iPrONO-d7) and (1,3-Pr(ONO)2)" suggests that the modeled values for BOTH these precursors are plotted, while in fact the model was apparently not run for the latter precursor (this goes back to my previous comment).

We modified the Figure 4 caption as follows:

"OH_{exp} values measured as a function of I_{369} following photolysis of perdeuterated isopropyl nitrite (iPrONO-d_7) and 1,3-propyl dinitrite (1,3-Pr$(ONO)_2$). Modeled OH_{exp} values obtained from **OFR369-i(iPrONO-d_7)** and OFR369-i(iPrONO) (Fig. 2d) are shown for reference...."

R2.18): Sections 3.3.1 and 3.3.2: are these sub-sections relevant to their parent section 3.3? The parent section title only mentions (iPrONO-d7) and (1,3-Pr(ONO)2). In fact, are these subsections even important enough to be placed in this part of the manuscript? There was no prior discussion of why MeONO and HFiPrONO are important OH precursors. These sub-sections abruptly build up the importance of these two precursors, and then rapidly declare that they are not suitable precursors in the OFR. The narrative flows smoother going directly from experimentally measuring OHexp to setting up estimation equations i.e., from P8 L33 directly to P9 L27. I suggest moving 3.3.1 and 3.3.2 to the end of the manuscript or to the SI.

We moved Section 3.3.1 (MeONO), Section 3.3.2 (now HONO, per reply to R2.1), and Section 3.3.3 (HFiPrONO) to a new Section 3.5 titled: "Anticipated performance of alternative high-NO_x HO_x precursors in OFRs"

R2.19): Sections 3.2 and 3.3 are really hitting the same hammer (how much OHexp is generated from precursor X) on different nails (X = iPrONO, deuterated iPrONO, etc.). I don't see why they need to be separate sections.

We prefer to maintain separate sections for discussion of iPrONO, which presumably will be more widely used, and synthesized alkyl nitrites, which we assume will be used by advanced users. We instead combined the current Sections 3.1 and 3.2 into a single section 3.1 titled "OH_{exp} and NO_x generated from iPrONO photolysis" with subsections 3.1.1 "Effect of photolysis

wavelength" and 3.1.2 "Effect of alkyl nitrite concentration".

R2.20): Figure S7b is missing a 1:1 line.

We added the 1:1 line.

R2.21): P10 L18: NO2 needs a subscript.

We added the subscript.

R2.22): P11 L5: OFR operation details (flow rate, etc.) should be described in the Section 2.3. Also, amount of α-pinene injected into OFR should be mentioned to give a sense of the OHR.

We moved some content from P11, L5 to Section 2.3, which now reads as follows:

"In a separate set of experiments, mass spectra of gas-phase α-pinene photooxidation products were obtained with an Aerodyne high-resolution time-of-flight chemical ionization mass spectrometer (Bertram et al., 2011) using nitrate as the reagent ion (NO_3^--HRToF-CIMS, hereafter abbreviated as NO_3^--CIMS) (Eisele and Tanner, 1993; Ehn et al., 2012). [...] The NO_3^--CIMS sampled the reactor output at 10.5 L min^{-1}. α-Pinene oxidation products were detected as adducts ions of NO_3^-. **In these experiments, the reactor was operated with a residence time of approximately 80 sec to accommodate the undiluted NO_3^--CIMS inlet flow requirement. OFR369-i(iPrONO) and OFR369-i(iPrONO-d_7) were operated using I_{369}= 6.5×10^{15} photons cm^{-2} s^{-1} and >7 ppm alkyl nitrite. In these experiments, α-pinene was evaporated into the carrier gas by flowing 1 sccm N_2 through a bubbler containing liquid α-pinene. Assuming the N_2 was saturated with α-pinene vapor, we estimate ~500 ppb α-pinene was introduced to the OFR based on its vapor pressure at room temperature and known dilution ratio into the main carrier gas. In a separate experiment, OFR254-iN_2O was operated using I_{254}= 3.2×10^{15} photons cm^{-2} s^{-1} + 5 ppm O_3 + 1% H_2O + 3.2% N_2O. Here, α-pinene was introduced by flowing 1 sccm N_2 of a gas mixture containing 150 ppm α-pinene in nitrogen (unavailable for the iPrONO photolysis experiments) into the main carrier gas.**".

R2.23): P11 L11: compound nomenclature is missing some subscripts.

We added missing subscripts to "$[(NO_3)C_7H_9NO_8^-]$" and "$[(NO_3)C_7H_{11}NO_8^-]$"

R2.24): P11 L20: this is a cool finding but does not readily jump out in Figure 5. I suggest adding a fourth panel showing a difference between the 5b and 5c (or 5a) spectra and zooming in the m/z scale to show the just a few –OD containing sticks (e.g., from m/z 310 to 360).

We implemented the reviewer's suggestion (please see R2.6).

R2.25) Figure 5: There is enough empty space in each subfigure to include the dinitrite:nitrite ratio value. I suggest adding this in to quantify the "highest ratios observed in 5b" statement on P11 L24.

The revised figure has 6 panels and consequently less empty space to include the dinitrate:nitrate ratio. However, we modified the text to include the dinitrate fractions:

P11, L24: "Second, C_{10} dinitrates were present in all three spectra, with the highest dinitrate:nitrate **fractions** observed in Figures 5b **(0.090)** and 5c **(0.081) and the lowest dinitrate:nitrate fraction observed in Figure 5a** (**0.056**).

R2.26) Figure S7: units of OHexp are incorrect on both X- and Y-axes (s, not s-1).

We changed the units of OH_{exp} from molec cm^{-3} s^{-1} to molec cm^{-3} s.

References:

Peng, Z.; Day, D. A.; Ortega, A. M.; Palm, B. B.; Hu, W. W.; Stark, H.; Li, R.; Tsigaridis, K.; Brune, W. H.; Jimenez, J. L. Non-OH chemistry in oxidation flow reactors for the study of atmospheric chemistry systematically examined by modeling. Atmos. Chem. Phys. Discuss. 2015, 15 (17), 23543–23586.

Lambe, A. T.; Ahern, A. T.; Williams, L. R.; Slowik, J. G.; Wong, J. P. S.; Abbatt, J. P. D.; Brune, W. H.; Ng, N. L.; Wright, J. P.; Croasdale, D. R.; et al. Characterization of aerosol photooxidation flow reactors: Heterogeneous oxidation, secondary organic aerosol formation and cloud condensation nuclei activity measurements. Atmos. Meas. Tech. 2011, 4 (3), 445–461.

Yan, C.; Nie, W.; Äijälä, M.; Rissanen, M. P.; Canagaratna, M. R.; Massoli, P.; Junninen, H.; Jokinen, T.; Sarnela, N.; Häme, S. A. K.; et al. Source characterization of highly oxidized multifunctional compounds in a boreal forest environment using positive matrix factorization. Atmos. Chem. Phys. 2016, 16 (19), 12715–12731.

Massoli, P.; Stark, H.; Canagaratna, M. R.; Krechmer, J. E.; Xu, L.; Ng, N. L.; Mauldin, R. L.; Yan, C.; Kimmel, J.; Misztal, P. K.; et al. Ambient Measurements of Highly Oxidized Gas-Phase Molecules during the Southern Oxidant and Aerosol Study (SOAS) 2013. ACS Earth Sp. Chem. 2018, 2 (7), 653–672.

Anonymous Referee #3

Summary and Recommendation

Authors introduce a new method for investigating NOx-dependent SOA formation pathways in oxidation flow reactors (OFRs). The new method uses alkyl nitrite photolysis to generate OH

and NO2 with two different lights (254 nm and 369 nm). It is an improvement over previous methods used to study NOx-dependent SOA formation pathways in OFRs for three primary reasons. First, because it does not require extremely high levels of ozone and it does not produce nitrate radical as a by-product; both ozone and nitrate radical also contribute to oxidation of SOA precursors and their presence in the reactor creates major challenges for deconvolving contributions from the different oxidants. Second, it can be run with 369 nm lamps and avoid photolytic losses of SOA precursors that can occur with the more commonly used 254 nm lamps. Third, unlike batch reaction chamber studies which can only probe over timescales of hours to ~1 day, the OFR can be used to probe oxidative aging equivalent to multiple days. There were a number of challenges using the new method. First, the alkyl nitrites presented an interference in the NOx analyzer, and they had to use a photochemical model to estimate NOx in lieu of a direct measurement. Second, the NOx generated from alkyl nitrite photolysis introduced an interference in the SO2 analyzer and made it difficult to determine OH exposure. They corrected for this by performing an offline calibration relating SO2 decay and particulate sulfate to OH exposure.The technique does not achieve equivalent OH exposures longer than one day, but does appear to be a promising technique for OFR users to study high NOx SOA chemistry. This is particularly true for oxidation conditions using 369 nm lights. I recommend the manuscript for publication after the following comments are addressed.

R3.1) Elaborate on alkyl nitrite interference with NOx analyzer. Text says they attempted to correct for the interference “to no avail” (p.3, l. 22). What was the issue that prevented this correction?

Please see our response to similar R2.13.

R3.2) OH exposure calibration: not entirely clear how this calibration provided a measure of equivalent OH exposure from OH and NO2 generated from alkyl nitrites. It could be cleared up by better describing the link between Figure S4 and Figure¶ S5. The connection is lost by lack of clarity regarding the x-axis in Figure S4 and explicitly stating at the end of the paragraph how the relationship in Figure S5 is used to estimate OH exposure as presented in Figure S4. In Figure S4, does the x-axis “sulfate” refers to both SO2 decay in the gas-phase and sulfate measured in the particles with the ACSM? There is something missing in the description that connects how the researchers propose to then presumably use the ACSM sulfate measurement in the presence of alkyl nitrites to estimate initial SO2 (Figure S5) and then relate that back to OH exposure using the relationship shown in Figure S4.

Please see our response to similar R2.3b, including the revised Figure S4 which we are hopeful will provide the necessary clarification to the question raised by Reviewer 3 here.

R3.3) Section 2.4: Additional reactions included in the model and all input parameters, rate constants, etc. are stated very clearly. Thank you. Uncertainties for actinic flux and organic nitrite concentration were also discussed very clearly. This model is being used to estimate NO and NO2 because of the NOx analyzer interference from alkyl nitrites (Section 2.2). I did not see

an estimate of the uncertainty for NO and NO2 estimates. Please add those.

Section 2.4 listed estimates of uncertainties for the model inputs: pressure, temperature, [iPrONO], mean residence time, actinic flux, and absorption cross sections and bimolecular rate constants. Because the NO and NO_2 mixing ratios are model outputs, the propagated model uncertainties in model input parameters that influence [NO] and [NO_2] for the specific model scenarios are represented by the shaded regions in Figures 2 and 3.

R3.4) Figure 2: The explanation for lower OHexp values with 254 nm lights versus 350 nm and 369 nm was not very clear (page 7-8). In particular, elaborate on the concept, “Because σiPrONO;369 « σiPrONO;254 (Table 1), the effect of photolysis wavelength on [NO2] is proportional to σiPrONO, as expected” and how that relates to reduced OH exposure at 254 nm. The other explanation for reduced OHexp with 254 nm lights (decomposition of iC3H7O radical) is described in adequate detail, but it would help to better clarify the proportion of iPrONO that decomposes at this wavelength to provide more context for how significant this pathway is at the shorter wavelengths.

We attempted to clarify this point by modifying the text as shown in our response to reviewer comment R2.4.

R3.5) Section 3.4: OHexp and NO2 estimation equations If this section is going to be included in the main text of the results, the Figure S7 should also be included in the main text since that figure summarizes the main results from this section. Alternatively, the entire section could be moved to supplement. Can you clarify the significance of the results from this section somewhere in the text?

We moved Figure S7 to the main text of the revised manuscript. We modified the text as follows:

P9, L28: “Previous studies reported empirical OH_{exp} algebraic estimation equations for OFR185 and OFR254 (Li et al., 2015; Peng et al., 2015). **These equations parameterize OH_{exp} as a function of readily-measured experimental conditions, therefore providing a simpler alternative to detailed photochemical models that** aid**s** in experimental planning and analysis.”

R3.6) One of the goals was to identify the optimal range of conditions for using the new alkyl nitrite method. Can you state the recommended “optimal” conditions more clearly AND also put the OFR conditions within that range into context relative to atmospheric conditions, particularly for NO:NO2 ratios and RO2:HOx? Are there certain conditions that should particularly be avoided? Can you make those more clear as well?

We modified the text as follows:

P12, L16: “Here, we adapted alkyl nitrite photolysis for new OFR applications by characterizing

the photolysis wavelength, nitrite concentration, and nitrite composition that result in optimal HOx and NOx generation capabilities. **Based on our results, we recommend photolysis of 5-10 ppm alkyl nitrite at λ ~ 365-370 nm photolysis wavelength and >10^{15} photons cm^{-2} s^{-1} actinic flux. If the user has the resources to synthesize iPrONO-d_7, better performance is expected relative to iPrONO. Alkyl nitrite photolysis at λ = 254 nm is not recommended.** Taken together, OFR254/185-iN_2O and OFR369-i(iPrONO/iPrONO-d_7) are complementary methods that provide additional flexibility for NOx-dependent OFR studies. OFR369-i(iPrONO)/OFR369-i(iPrONO-d_7) generate high-NO_x photooxidation conditions ($NO:HO_2$ ≈10-10000; **$NO:NO_2$ ≈ 0.2-0.7).”**

R3.7) One of the stated benefits of OFRs in the intro is their ability to simulate “multiple days of equivalent atmospheric exposure.” (P. 2, L. 4). Looking at Figures 2-4, it does not appear the OFR was capable of obtaining more than 1 day equivalent OH exposure either using the alkyl nitrite technique. Can you comment on how this timescale compares with smog chamber experiments investigating similar NOx pathways?

We note that the text on P2, L4 (which is part of the introduction) refers to other versions of the OFR chemistry described in previous publications.

Otherwise, one of the goals of this work was to achieve HOx generation via photolysis of 1,1,1,3,3,3-hexafluoroisopropyl nitrite (HFiPrONO) because modeling suggested it is capable of simulating multiple days of OH exposure due to its extremely low OH reactivity. This detail was omitted from the discussions manuscript but we have added it to the revised manuscript to provide additional context. As described in the paper, we were unable to synthesize HFiPrONO, following literature methods.

We modified the text as follows:

P9, L15: “We **predict** that OFR369-i(HFiPrONO) should attain higher OH_{exp} than OFR369-i(iPrONO) and OFR369-i(iPrONO-d_7) due to similar photolysis rates (Andersen et al., 2003) and ~200 times lower OH reactivity of HFiPrONO/hexafluoroacetone relative to iPrONO/acetone (Atkinson et al., 1992; Tokuhashi et al., 1999). **Simple modeling calculations suggest that application of OFR369-i(HFiPrONO) may achieve up to a week of equivalent OH exposure.”**

P12, L21: “We anticipate that alkyl nitrite photolysis is suitable for the characterization of first-generation, high-NOx photooxidation products of most precursors, **at OH_{exp} comparable to environmental chambers investigating high-NO_x conditions.**”

R3.8) It would be helpful to see a direct comparison between OH exposure using the alkyl nitrite method versus other techniques that have been used to probe the high NOx pathway (for example, N2O addition).

We modified the text as shown in our response to the similar reviewer comment R1.1.

R3.9)P. 2, L. 28-30: alkyl nitrite were stored in amber vials and refrigerated until use. Can you clarify how long they can be stored and approximately how much time passed from synthesis to experimental use in these experiments?

We consulted with Pfaltz and Bauer, Inc., the company from which we obtained isopropyl nitrite. We received the following email response from a sales manager on 29 October 2018:

"Andy,

Per your request for the shelf life of our I10550, 2 years is a general guide.

We have seen 3 years if refrigerated and the container kept tightly closed away from moisture.

Regards,

Bob Milburn
Inside Sales Manager
Pfaltz & Bauer, Inc.
172 E. Aurora St.
Waterbury, CT 06708
tel 203-574-0075 X102
fax 203-574-3181
bobm@pfaltzandbauer.com
www.pfaltzandbauer.com"

We modified the text as follows:

"The resulting clear yellow liquid was dried over sodium sulfate, neutralized with excess sodium bicarbonate, and then stored in amber vials and refrigerated at 4°C until use **(within one week of synthesis in this work)**. **Under these storage conditions, the nominal shelf life of isopropyl nitrite and similar organic nitrites is approximately 2 years (B. Milburn, personal communication, 29 October 2018).** "

HO_x and NO_x production in oxidation flow reactors via photolysis of isopropyl nitrite, isopropyl nitrite-d_7, and 1,3-propyl dinitrite at λ = 254, 350, and 369 nm

Andrew Lambe[1], Jordan Krechmer[1], Zhe Peng[2], Jason Casar[3], Anthony Carrasquillo[4], Jonathan Raff[5], Jose Jimenez[2], and Douglas Worsnop[1,6]

[1]Center for Aerosol and Cloud Chemistry, Aerodyne Research Inc., Billerica, MA, USA
[2]Dept. of Chemistry and Cooperative Institute for Research in Environmental Sciences (CIRES), University of Colorado, Boulder, CO, USA
[3]Dept. of Chemistry, Harvey Mudd College, Claremont, CA, USA
[4]Dept. of Chemistry, Williams College, Williamstown, MA, USA
[5]School of Public and Environmental Affairs, Indiana University, Bloomington, IN, USA
[6]Dept. of Physics, University of Helsinki, Helsinki, FI

Correspondence: Andrew T. Lambe (lambe@aerodyne.com), Zhe Peng (zhe.peng@colorado.edu)

Abstract. Oxidation flow reactors (OFRs) are an emerging technique for studying the formation and oxidative aging of organic aerosols and other applications. In these flow reactors, hydroxyl radicals (OH), hydroperoxyl radicals (HO_2), and nitric oxide (NO) are typically produced in the following ways: photolysis of ozone (O_3) at ~~t~~λ = 254 nm, photolysis of H_2O at λ = 185 nm, and via reactions of $O(^1D)$ with H_2O and nitrous oxide (N_2O); $O(^1D)$ is formed via photolysis of O_3 at λ = 254 nm and/or N_2O at λ = 185 nm. Here, we adapt a complementary method that uses alkyl nitrite photolysis as a source of OH via its production of HO_2 and NO followed by the reaction NO + HO_2 $\rightarrow$ NO_2 + OH. We present experimental and model characterization of the OH exposure and NO_x levels generated via photolysis of C_3 alkyl nitrites (isopropyl nitrite, perdeuterated isopropyl nitrite, 1,3-propyl dinitrite) in the Potential Aerosol Mass (PAM) OFR as a function of photolysis wavelength (λ = 254 to 369 nm) and organic nitrite concentration (0.5 to 20 ppm). We also apply this technique in conjunction with chemical ionization mass spectrometer measurements of multifunctional oxidation products generated following the exposure of α-pinene to HO_x and NO_x obtained using both isopropyl nitrite and O_3 + H_2O + N_2O as the radical precursors.

1 Introduction

Hydroxyl (OH) radicals govern the concentrations of most atmospheric organic compounds, including those that lead to secondary organic aerosol (SOA) formation. The relative importance of different primary OH precursors varies in different parts of the atmosphere, and may include contributions from $O(^1D)$-H_2O reactions, hydrogen peroxide (H_2O_2), methyl peroxide (CH_3OOH), nitrous acid (HONO) photolysis, and ozone-alkene reactions. Additionally, ozone-hydroperoxy (HO_2) reactions and NO-HO_2 reactions recycle HO_2 back to OH (Mao et al., 2009; Lee et al., 2016). For decades, a handful of radical precursors have been used to generate OH radicals in the laboratory to initiate SOA production under controlled conditions. Environmental chambers most commonly photolyze nitrous acid (HONO), methyl nitrite (CH_3ONO), or hydrogen peroxide

(H_2O_2) at $\lambda > 310$ nm to mimic SOA production, over experimental timescales of hours to days, simulating up to 2 days of equivalent atmospheric exposure (Atkinson et al., 1981; Matsunaga and Ziemann, 2010; Chhabra et al., 2011; Finewax et al., 2018).

Oxidation flow reactors (OFRs) photolyze H_2O and O_3 at λ = 185 and 254 nm over experimental timescales of minutes, simulating multiple days of equivalent atmospheric exposure (Lambe et al., 2012; Peng et al., 2015). Recent application of $O(^1D)$ + H_2O + N_2O reactions to study NO_x-dependent SOA formation pathways facilitated characterization of oxidation products generated over a range of low- to high-NO_x conditions (Lambe et al., 2017; Peng et al., 2018). Potential limitations of the method include: (1) Inability to unambiguously deconvolve contributions from multiple oxidants (O_3, OH, NO_3), which may compete with each other under certain conditions and for specific unsaturated precursors; (2) required use of 254 nm photolysis, which may enhance photolytic losses that compete with OH oxidation, especially for species that are characterized by strong absorption/quantum yield at 254 nm and low OH reactivity (Peng et al., 2016); (3) optimal high-NO_x application at OH exposures corresponding to multiple equivalent days of oxidative aging rather than one day or less.

Here, we adapt a complementary method that uses alkyl nitrite photolysis to generate an alkoxy radical (RO•) and NO. In the presence of air, RO reacts with O_2 to generate a carbonyl product (R'O) and a hydroperoxyl (HO_2) radical, and NO and HO_2 subsequently react to generate OH and NO_2. Using this method, O_3 is not required to generate OH radicals, and insignificant amounts of O_3 or NO_3 are generated as byproducts. We present experimental and model characterization of OH and NO_x levels that are generated as a function of photolysis wavelength, and organic nitrite concentration and composition. We furthermore carried out chemical ionization mass spectrometer measurements to compare nitrogen-containing photooxidation products obtained from the reaction of α-pinene with radicals generated via alkyl nitrite photolysis or the $O(^1D)$ + H_2O + N_2O reaction.

2 Experimental

2.1 Alkyl nitrite preparation

Figure 1 shows molecular structures of the alkyl nitrites that were used. Isopropyl nitrite (iPrONO; Pfaltz and Bauer, >95% purity) was used without additional purification. Perdeuterated isopropyl nitrite (iPrONO-d_7) and 1,3-propyl dinitrite [1,3-$Pr(ONO)_2$] were synthesized from the action of HONO on isopropanol-d_8 or 1,3-propanediol, respectively, as described elsewhere (Noyes, 1933; Andersen et al., 2003; Shuping et al., 2006; Carrasquillo et al., 2014). Briefly, sodium nitrite (>99.999%, Sigma-Aldrich) and the alcohol were combined in a 1.1:1.0 molar ratio and stirred with a magnetic stirrer inside a round bottom flask. Sulfuric acid was added dropwise to the flask – thereby generating HONO upon reaction with sodium nitrite – until a 0.5:1.0 acid:alcohol molar ratio was achieved. The resulting clear yellow liquid was dried over sodium sulfate, neutralized with excess sodium bicarbonate, and then stored in amber vials and refrigerated at 4^{o}C until use (within 1 week of synthesis in this work). Under these storage conditions, the nominal shelf life of iPrONO and similar organic nitrites is approximately 2 years (B. Milburn, personal communication, 29 October 2018).

A syringe pump was used to introduce iPrONO, iPrONO-d_7, and 1,3-$Pr(ONO)_2$ through a 10.2 cm length of 0.0152 cm ID teflon tubing at liquid flow rates ranging from 0.016 to 0.63 μL min^{-1}. The liquid organic nitrite was evaporated into a 1 L min^{-1} N_2 carrier gas at the end of the tubing. The flow containing organic nitrite vapor was then mixed with a 7 L min^{-1} synthetic air carrier gas at the reactor inlet.

The organic nitrite mixing ratio entering the reactor, r_{RONO}, was equal to $\frac{Q_{RONO,g}}{Q_{carrier}}$, where $Q_{RONO,g}$ was the volumetric flow rate of organic nitrite vapor (L min^{-1}) and $Q_{carrier}$ was the volumetric flow rate of carrier gas (L min^{-1}). $Q_{RONO,g}$ was calculated using the ideal gas law as applied by Liu et al. (2015):

$$Q_{RONO,g} = Q_{RONO,l} \times \frac{\rho}{MW} \times \frac{RT}{P} \times 0.01 \quad (1)$$

where $Q_{RONO,l}$ (μL min^{-1}) is the volumetric flow of organic nitrite liquid, ρ (g cm^{-3}) and MW (g mol^{-1}) are the organic nitrite liquid density and molecular weight, *R* (8.314 J mol^{-1} K^{-1}) is the universal gas constant, *T* (K) is temperature, *P* (hPa) is pressure, and 0.01 is a lumped pressure, volume and density unit conversion factor.

2.2 Alkyl nitrite photolysis

Alkyl nitrites were photolyzed inside a Potential Aerosol Mass (PAM) oxidation flow reactor (Aerodyne Research, Inc.), which is a horizontal 13.3 L aluminum cylindrical chamber (46 cm long × 22 cm ID) operated in continuous flow mode (Lambe et al., 2017), with 5.1±0.3 L min^{-1} flow through the reactor unless stated otherwise. The relative humidity (RH) in the reactor was controlled in the range of 31-63% at 21-32° C ~~, corresponding to~~ using a Nafion humidifier (Perma Pure LLC), with corresponding H_2O volumetric mixing ratios of approximately 1.5-1.7%. Four UV lamps centered at λ = 254 nm (GPH436T5L; Light Sources, Inc.), 350 nm (F436T5/BL/4P-350; Aerodyne Research, Inc.), or 369 nm (F436T5/BLC/4P-369; Aerodyne Research, Inc.) were used. Emission spectra obtained from the primary manufacturer (Light Sources, Inc. or LCD Lighting, Inc.) are shown in Figure S1. A fluorescent dimming ballast (IZT-2S28-D, Advance Transformer Co.) was used to regulate current applied to the lamps. The UV irradiance was measured using a photodetector (TOCON-GaP6, sglux GmbH) and was varied by changing the control voltage applied to the ballast between 1.6 and 10 VDC.

NO and NO_2 mixing ratios were measured using a NO_x analyzer (Model 405 nm, 2B Technologies), which quantified [NO_2] (ppb) from the measured absorbance at λ = 405 nm, and [NO] (ppb) by reaction with O_3 to convert to NO_2. Alkyl nitrites introduced to the reactor with the lamps turned off consistently generated signals in the both NO and NO_2 measurement channels of the NO_x analyzer, possibly due to impurities ~~.~~ and/or species generated via iPrONO + O_3 reactions inside the analyzer. For example, background NO and NO_2 mixing ratios increased from 0 to 1526 ppb and 0 to 1389 ppb as a function of injected [iPrONO] = 0 to 18.7 ppm with the lamps off (Figure S2). We attempted to correct [NO] and [NO_2] for this apparent alkyl nitrite interference by subtracting background signals measured in the presence of alkyl nitrite with lamps off, to no avail, because background signals (alkyl nitrite present with lamps off) were large compared to signals obtained with alkyl nitrite present with lamps on. Instead, we constrained [NO] and [NO_2] using the photochemical model discussed in Section 2.4.

2.2.1 Actinic flux calibration

To quantify the actinic flux I in the reactor for each lamp type, we measured the rate of NO_2 photolysis as a function of UV irradiance (Figure S4). Measurements were conducted in the absence of oxygen to avoid O_3 formation. The first-order NO_2 photolysis rate (j_{NO_2}) was calculated using Equation 2:

$$j_{NO_2} = \ln\left(\frac{NO_{2,\tau}}{NO_{2,0}}\right)\frac{1}{\tau_{NO_2}} \quad (2)$$

where $NO_{2,0}$ and $NO_{2,\tau}$ were the steady-state NO_2 mixing ratios measured at the exit of the reactor with the lamps turned off and on, respectively. The mean NO_2 residence time in the reactor, τ_{NO_2}, was characterized using 10-second pulsed inputs of NO_2. To mimic the effect of axial dispersion induced by temperature gradients from the lamps being turned on (Lambe et al., 2011; Huang et al., 2017), residence time distributions were measured in the presence of four lamps centered at λ = 658 nm (F436T5/4P-658; Aerodyne Research, Inc.), where the NO_2 quantum yield is zero (Gardner et al., 1987). NO_2 residence time distributions are shown in Figure S3, where τ_{NO_2} ranged from 120 $\pm$ 34 s ($\pm 1\sigma$; lamps off) to 98 $\pm$ 63 s ($\pm 1\sigma$; lamps on) in a manner that is consistent with previous observations (Lambe et al., 2011; Huang et al., 2017). Assuming τ_{NO_2} = 98 s, maximum j_{NO_2} values were 0.12, 0.36, and 0.50 min^{-1} following photolysis at full lamp power at λ = 254, 350, and 369 nm, respectively.

Corresponding I_{254}, I_{350}, and I_{369} values were calculated using a photochemical model implemented in the KinSim ~~(Peng et al., 2015)~~ chemical kinetics solver (Peng et al. (2015); implemented within Igor Pro 7, Wavemetrics Inc.) that incorporated the following reactions:

$$NO_2 + h\nu \rightarrow NO + O(^3P) \quad (R1)$$

$$O(^3P) + NO \rightarrow NO_2 \quad (R2)$$

$$O(^3P) + NO_2 \rightarrow NO_3 \quad (R3)$$

$$O(^3P) + NO_2 \rightarrow NO + O_2 \quad (R4)$$

NO_2 absorption cross sections were averaged across the 254, 350, and 369 nm lamp emission spectra, respectively (Table 1) (Atkinson et al., 2004) and input to the model. Maximum I_{254} = 8.6$\times$ 10^{16} photons cm^{-2} s^{-1}, I_{350} = 6.3 $\times$ 10^{15} photons cm^{-2} s^{-1}, and I_{369} = 6.5 $\times$ 10^{15} photons cm^{-2} s^{-1}, respectively were obtained. While I_{350} and I_{369} values were in agreement with values calculated from lamp manufacturer specifications (I_{350} = 5.8 $\times$ 10^{15} and I_{369} = 6.2 $\times$ 10^{15} photons cm^{-2} s^{-1}) within uncertainties, I_{254} obtained from our calibration was $\sim$13 times larger than expected. We hypothesize that this discrepancy was due to the presence of additional minor mercury lines (e.g. $\lambda \sim$ 313, 365, 405) that induce NO_2 photolysis and that were not fully accounted for using Eq. 2 or the manufacturer spectra (Figure S1). Thus, we instead assume maximum I_{254} = 6.5$\times$ 10^{15} photons cm^{-2} s^{-1} based on manufacturer specifications.

2.2.2 OH exposure calibration

The OH exposure (OH_{exp}) obtained from alkyl nitrite photolysis, that is, the product of the OH concentration and mean residence time, was calculated from the addition of between 280 and 420 ppb SO_2 at the reactor inlet. Over the course of these experiments, NO_x generated from alkyl nitrite photolysis significantly interfered with the SO_2 mixing ratio measured with an SO_2 analyzer (Model 43i, Thermo Scientific)~~.~~; a representative example is shown in Fig. S5. To circumvent this issue, we measured the initial SO_2 mixing ratio, $[SO_{2,0}]$, prior to alkyl nitrite photolysis, then used an Aerosol Chemical Speciation Monitor ~~(Ng et al., 2011) (~~(ACSM; Aerodyne Research, Inc.) to measure the concentration of particulate sulfate generated from SO_2 + OH reactions.

To relate the measured $[SO_{2,0}]$ and sulfate to OH_{exp}, we conducted an offline calibration where 493 ppb SO_2 was added to the reactor and OH was generated via $O_3 + h\nu_{254} \rightarrow O(^1D) + O_2$ followed by $O(^1D) + H_2O \rightarrow 2OH$ in the absence of NO_x ("OFR254" mode). The reactor was operated at the same residence time and humidity that was used in alkyl nitrite experiments~~.~~, although we note that humidity will not change the response of the ACSM to sulfuric acid aerosols. Because no particulate ammonia was present aside from trace background levels, we assumed an ACSM collection efficiency of unity for the sulfate particles. SO_2 decay and particulate sulfate formation were measured across a range of UV irradiance and $[O_3]$, from which a calibration equation relating sulfate to OH_{exp} was obtained (Figure S6) and applied to alkyl nitrite photolysis experiments. In a separate experiment conducted with 2.2 ppm of iPrONO input to the reactor at I_{369} = 6.5×10^{15} photons cm^{-2} s^{-1}, we verified that the mass of particulate sulfate detected by the ACSM responded linearly to a change in the input mixing ratio of SO_2 between 200 and 473 ppb (Figure S7). This suggests that the sulfate particles were large enough for efficient transmission through the inlet lens of the ACSM across the range of OH_{exp} used in our experiments. While not applicable in this work, we note that heterogeneous uptake of SO_2 onto organic aerosol may bias OH exposure measurements (Ye et al., 2018).

2.3 Chemical Ionization Mass Spectrometer (CIMS) measurements

In a separate set of experiments, mass spectra of gas-phase α-pinene photooxidation products were obtained with an Aerodyne high-resolution time-of-flight chemical ionization mass spectrometer ~~(Bertram et al., 2011)~~ using nitrate as the reagent ion (NO_3^--HRToF-CIMS, hereafter abbreviated as NO_3^--CIMS) (Eisele and Tanner, 1993; Ehn et al., 2012). Nitrate (NO_3^-) and its higher-order clusters (e.g. $HNO_3NO_3^-$) generated from X-ray ionization of HNO_3 were used as the reagent due to their selectivity to highly oxidized organic compounds, including species that contribute to SOA formation (Ehn et al., 2014; Krechmer et al., 2015; Lambe et al., 2017). The NO_3^--CIMS sampled the reactor output at 10.5 L min^{-1}. α-Pinene oxidation products were detected as adducts ions of NO_3^-. In these experiments, the reactor was operated with a residence time of approximately 80 sec to accommodate the undiluted NO_3^--CIMS inlet flow requirement. OFR369-i(iPrONO) and OFR369-i(iPrONO-d_7) were operated using I_{369} = 6.5×10^{15} photons cm^{-2} s^{-1} and >7 ppm alkyl nitrite; in these experiments, α-pinene was evaporated into the carrier gas by flowing 1 sccm N_2 through a bubbler containing liquid α-pinene. Assuming the N_2 flow was saturated with α-pinene vapor, we estimate ~500 ppb α-pinene was introduced to the OFR based on its vapor pressure at room temperature and known dilution ratio into the main carrier gas. In a separate experiment, OFR254-iN_2O was operated

using I_{254} = 3.2×10^{15} photons cm^{-2} s^{-1} and 5 ppm O_3 + 1% H_2O + 3.2% N_2O. Here, α-pinene was introduced by flowing 1 sccm of a gas mixture containing 150 ppm α-pinene in N_2 into the main carrier gas (this gas mixture was unavailable for the iPrONO photolysis experiments); the calculated α-pinene mixing ratio that was introduced to the OFR was ~ 16 ppb.

2.4 Photochemical model

We used the KinSim OFR photochemical model ~~(Peng et al., 2015; Peng and Jimenez, 2017)~~ to calculate concentrations of radical/oxidant species produced (Peng et al., 2015; Peng and Jimenez, 2017) . In addition to NO + HO_2 → OH + NO_2 and other reactions included in Peng and Jimenez (2017), the following reactions were added for this study:

$$\mathrm{iPrONO} + h\nu \rightarrow \mathrm{iC_3H_7O\bullet} + \mathrm{NO} \quad \text{(R5)}$$

$$\mathrm{iPrONO} + h\nu \rightarrow \mathrm{CH_3CHO} + \mathrm{CH_3\bullet} + \mathrm{NO} \quad \text{(R6)}$$

$$\mathrm{CH_3\bullet} + \mathrm{O_2} \rightarrow \mathrm{CH_3O_2\bullet} \quad \text{(R7)}$$

$$\mathrm{iC_3H_7O\bullet} + \mathrm{O_2} \rightarrow \mathrm{(CH_3)_2C(O)} + \mathrm{HO_2} \quad \text{(R8)}$$

$$\mathrm{(CH_3)_2CO} + \mathrm{OH} \rightarrow \mathrm{Products} \quad \text{(R9)}$$

$$\mathrm{iPrONO} + \mathrm{OH} \rightarrow \mathrm{(CH_3)_2C(O)} + \mathrm{NO} \quad \text{(R10)}$$

$$\mathrm{CH_3CHO} + \mathrm{OH} \rightarrow \mathrm{CH_3CO\bullet} + \mathrm{H_2O} \quad \text{(R11)}$$

$$\mathrm{CH_3CO\bullet} + \mathrm{O_2} \rightarrow \mathrm{CH_3C(O)O_2\bullet} \quad \text{(R12)}$$

$$\mathrm{CH_3C(O)O_2\bullet} + \mathrm{NO} \rightarrow \mathrm{CH_3\bullet} + \mathrm{NO_2} + \mathrm{CO_2} \quad \text{(R13)}$$

$$\mathrm{CH_3O_2\bullet} + \mathrm{NO} \rightarrow \mathrm{CH_3O\bullet} + \mathrm{NO_2} \quad \text{(R14)}$$

$$\mathrm{CH_3O\bullet} + \mathrm{O_2} \rightarrow \mathrm{HCHO} + \mathrm{HO_2} \quad \text{(R15)}$$

$$\mathrm{HCHO} + \mathrm{OH} \rightarrow \mathrm{HCO\bullet} + \mathrm{H_2O} \quad \text{(R16)}$$

$$\mathrm{HCO\bullet} + \mathrm{O_2} \rightarrow \mathrm{CO} + \mathrm{HO_2} \quad \text{(R17)}$$

Model input parameters included pressure, temperature, [H_2O], [iPrONO], mean residence time, actinic flux, and absorption cross sections and bimolecular rate constants shown in Table 1. We assumed the quantum yield of Reaction R5 to be ~~0.5(Raff and Finlayson-Pitts, 2010)and that~~ 0.50 above 350 nm (Raff and Finlayson-Pitts, 2010). We assumed the quantum yield of Reaction R6 to be 0.04 above 350 nm (value for *t*-butyl nitrite) (Calvert and Pitts, 1966), suggesting minimal influence of CH_3O_2 and $CH_3C(O)O_2$ that are generated via Reactions R7, R10, and R11 following iPrONO decomposition to CH_3 and CH_3CHO via Reaction R6. At 254 nm, ~~Calvert and Pitts (1966) estimated the~~ the influence of CH_3O_2 and $CH_3C(O)O_2$ on ensuing photochemistry may be more significant.This is due to a higher quantum yield of Reaction R6 at 254 nm, which is estimated to be 0.86 under vacuum ~~. To account for some effect of collisional deactivation that prevent~~ (Calvert and Pitts, 1966). Assuming that all 254 nm photons initiate photolysis, the quantum yield of Reaction R5 is 0.14. Due to collisional deactivation at 1 atm that prevents *i*-$C_3H_7O\bullet$ decomposition~~at~~ , the quantum yield of Reaction R5 at λ = 254 nm and 1 atm ~~, we assumed a~~

~~lower quantum yield (0.73) for Reaction R6 and the~~ is expected to be higher than 0.14. Because quantum yield measurements were unavailable at these conditions, we applied an upper limit quantum yield of 0.50 as applicable at λ >350 nm and 1 atm (Raff and Finlayson-Pitts, 2010). We calculated a corresponding nominal quantum yield of 0.32 by averaging the lower and upper limit values of 0.14 and 0.50, resulting in a quantum yield of ~~Reaction R5 to be 0.27 at 254 nm.~~ 0.68 for Reaction R6.

We assumed that the residence time distribution of iPrONO in the reactor was similar to the residence time distribution of NO_2. To model iPrONO photolysis at λ = 254 nm, we extended the range of previously-measured σ_{iPrONO} values by measuring the gas phase absorption cross sections of iPrONO (purified via four freeze-pump-thaw cycles prior to measurement) down to λ = 220 nm using a custom-built absorption cell (Raff and Finlayson-Pitts, 2010). Results at λ = 220 to 436 nm are shown in Figure S1 and are in agreement with previous work (Raff and Finlayson-Pitts, 2010) over the range of overlap at λ = 300 to 450 nm.

~~Measured quantum yields are unavailable for Reaction R5 at 254 nm or for Reaction R6 at 1 atm. There are~~ To account for uncertainties associated with the assumptions we made for ~~these quantum yields. To properly take into account these uncertainties~~quantum yield values, as well as uncertainties in other kinetic parameters, temperature, residence time, actinic flux, and organic nitrite concentration, we performed Monte Carlo uncertainty propagation (BIPM et al., 2008) as described previously (Peng et al., 2015; Peng and Jimenez, 2017). All uncertain kinetic parameters were assumed to follow log-normal distributions unless stated otherwise below. Uncertainties in rate constants and cross sections newly included in this study were adopted from Burkholder et al. (2015) if available. The relative uncertainty in the rate constant of Reaction R13 was estimated to be 40% based on the dispersion of rate constant measurements of published RO_2 + NO reactions. We assumed the random samples of the quantum yields of Reactions R5 and R6 at 254 nm and Reaction R6 at 369 nm followed uniform distributions in the range of [~~0.6~~0.50, 0.86], [0.14, 0.50] and [0, ~~0.2~~0.20], respectively. We assumed uncertainties of 5 K and 20 s in temperature and residence time (normal distributions assumed), respectively, and relative uncertainties of 50%, 100%, and 25% in actinic flux at 369 nm, actinic flux at 254 nm, and organic nitrite concentration, respectively.

3 Results and Discussion

We first characterized OH_{exp} and NO_x by separately varying the photolysis wavelength (Sect. 3.1.1) and input organic nitrite concentration to the reactor (Sec. 3.1.1), with the goal of identifying optimal OFR conditions for OH and NO_x generation via iPrONO photolysis. Second, we synthesized novel alkyl nitrites and compared their performance to iPrONO (Sec. 3.2). Third, we parameterized OH_{exp} and NO_2 production in a set of algebraic equations to guide selection of OFR experimental conditions. Finally, we compared NO_3^--CIMS spectra of photooxidation products generated from reaction of α-pinene with radicals produced via alkyl nitrite photolysis and $O(^1D)$ + H_2O + N_2O reactions.

3.1 OH_{exp} and NO_x generated from iPrONO photolysis~~: Effect of photolysis wavelength~~

3.1.1 Effect of photolysis wavelength

Figure 2 shows OH_{exp}, [NO], and [NO_2] obtained as a function of actinic flux following photolysis of 1.9 ppm of iPrONO injected into the reactor at λ = 254, 350, or 369 nm. These systems are hereafter designated as OFR254-i(iPrONO), OFR350-i(iPrONO), and OFR369-i(iPrONO), respectively; similar nomenclature is adapted for other alkyl nitrites. In these notations, the numbers following "OFR" are the photolysis wavelengths (in nm), and the "i" preceding the parentheses means initial injection of the radical precursor compound noted in the parentheses. Modeled OH_{exp}, NO, and NO_2 values for the OFR254-i(PrONO) and OFR369-i(PrONO) modes are shown in Figure 2 at the same nominal operating conditions.

At a fixed photolysis wavelength, OH_{exp}, NO, and NO_2 increased with increasing actinic flux. Measured and modeled OH_{exp} values were in agreement within uncertainties at λ = 369 nm. At λ = 254 nm, model OH_{exp} results were higher than the measurements, perhaps due to uncertainty in assumptions that were necessary to model OFR254-i(iPrONO) (Section 2.4). ~~At fixed *I*, modeled NO values attained via OFR369-i(iPrONO) were higher than via OFR254-i(iPrONO), and modeled~~ Higher NO_2 ~~values attained via OFR254-i(iPrONO) were higher than OFR369-i(iPrONO). Because $\sigma_{iPrONO,369} << \sigma_{iPrONO,254}$ (Table 1), the effect of photolysis wavelength on~~ concentrations were modeled at λ = 254 nm than at λ = 369 nm because more iPrONO was photolyzed and the NO_2 ~~is proportional to σ_{iPrONO}, as expected.~~ yield was only weakly dependent on the fate of *i*-C_3H_7O•. For example, NO is converted to NO_2 either via reaction with HO_2 obtained via Reaction R5 or CH_3O_2• and $CH_3C(O)O_2$• obtained via Reaction R6. However, the effect of photolysis wavelength on NO and OH_{exp} was different~~:~~ . Specifically, the highest NO concentration and OH_{exp} was achieved via OFR369-i(iPrONO). OH_{exp} achieved via OFR369-i(iPrONO) was slightly higher than OH_{exp} attained using OFR350-i(iPrONO), likely because photolysis of both iPrONO and NO_2, whose reaction with OH suppresses OH_{exp}, is more efficient at λ = 369 nm than at λ = 350 nm (Figure S1 ~~b~~ and Table 1). Further, the ~~OH yield attained~~ NO and OH yields achieved via OFR254-i(iPrONO) ~~is presumably~~ were suppressed due to significant (>73%) decomposition of iC_3H_7O• (Calvert and Pitts, 1966). The dependence of OH, NO and NO_2 on the quantum yields of Reactions R5 and R6 was confirmed by sensitivity analysis of uncertainty propagation inputs and outputs as described in Section 2.4. OH_{exp} and NO were strongly anticorrelated with the quantum yield of Reaction R6, whereas the correlation between NO_2 and the quantum yield of Reaction R6 was negligible.

The products of this decomposition, i.e., CH_3CHO and CH_3•, both have adverse effects with regard to our experimental goals: CH_3CHO is reactive toward OH and can thus suppress OH; the RO_2• formed through this reaction, $CH_3C(O)O_2$•, consumes NO and generates NO_2 but does not generate OH; CH_3• rapidly converts to CH_3O_2•, which also consumes NO and generates NO_2 but does not directly produce OH. Importantly, Figure 2 suggests that it is preferable to photolyze alkyl nitrates at λ > 350 because optimal OH_{exp} and NO:NO_2 were attained via OFR369-i(iPrONO). Moreover there is added risk for significant unwanted photolysis of organics via OFR254-i(iPrONO) (Peng et al., 2016).

3.2 ~~OH_{exp} and generated from iPrONO photolysis: effect of alkyl nitrite concentration~~

3.1.1 Effect of alkyl nitrite concentration

Figure 3 shows measured ~~and modeled~~ OH_{exp} and modeled NO_x concentrations obtained from photolysis of 0.5 to 20 ppm iPrONO at $I_{369} \approx 7\times10^{15}$ photons cm^{-2} s^{-1}. [NO] and [NO_2] increased with increasing [iPrONO], as expected. For [iPrONO] $\leq$ 5 ppm, OH_{exp} increased with increasing [iPrONO] because the rate of OH production increased faster than the rate of OH destruction from reaction with iPrONO and NO_2. ~~For~~ The model results showed that for [iPrONO] $>$ 5 ppm, the opposite was true and OH_{exp} plateued or decreased. A maximum OH_{exp} = 7.8×10^{10} molecules cm^{-3} s was achieved via photolysis of 10 ppm iPrONO, with corresponding modeled [NO] and [NO_2] values of 148 and 405 ppb respectively. Modeled NO_3 concentrations were negligible in OFR369-i(iPrONO) ($\leq$ 1 ppt) because there was no O_3 present and NO_3 production via HNO_3 + OH $\rightarrow$ NO_3 + H_2O reactions was insignificant.

3.2 OH_{exp} generated from photolysis of perdeuterated iPrONO and 1,3-propyl dinitrite

Although OH_{exp} = 7.8×10^{10} molecules cm^{-3} s (approximately 0.6 d of equivalent atmospheric OH exposure) may be suitable for some OFR applications, it may be insufficient to simulate multigenerational oxidative aging of precursors with OH rate constants slower than $\sim$ 10^{-11} cm^3 $molecule^{-1}$ s^{-1}. We attempted to synthesize three C_3 alkyl nitrites that we hypothesized could generate higher OH_{exp} than iPrONO: perdeuterated isopropyl nitrite (iPrONO-d_7), 1,3-propyl dinitrite [1,3-Pr$(ONO)_2$], and hexafluoroisopropyl nitrite (HFiPrONO). We successfully synthesized 1,3-Pr$(ONO)_2$ and iPrONO-d_7, but were unable to synthesize HFiPrONO (Sect. 3.5.3). Figure 4 shows OH_{exp} attained from photolysis of 1.2 ppm 1,3-Pr$(ONO)_2$ and 1.7 ppm iPrONO-d_7 as a function of I_{369}, along with the model output for OFR369-i(iPrONO) shown for reference. At these organic nitrite concentrations and I_{369} values, maximum OH_{exp} measurements were: 1.1×10^{11} (iPrONO-d_7), 4.0×10^{10} (iPrONO), and 1.8×10^{10} molecules cm^{-3} s [1,3-Pr$(ONO)_2$], respectively. At maximum I_{369} and after correcting for the different iPrONO, iPrONO-d_7 and 1,3-Pr$(ONO)_2$ concentrations that were used (Figure 3), $OH_{exp,iPrONO-d_7} \approx 2.9 \times OH_{exp,iPrONO}$ and $OH_{exp,1,3-Pr(ONO)_2} \approx 0.81 \times OH_{exp,iPrONO}$.

We hypothesize that higher OH_{exp} obtained from OFR369-i(iPrONO-d_7) relative to OFR369-i(iPrONO) was due to $\sim$2.6 times lower OH reactivity of iPrONO-d_7 relative to iPrONO (Nielsen et al., 1988, 1991) and 6 times lower OH reactivity of acetone-d_6 relative to acetone (Raff et al., 2005). This hypothesis is supported by the modeled OH_{exp} attained via OFR369-i(iPrONO-d_7), which is in agreement with measured OH_{exp} within uncertainties and is 41% higher than modeled OH_{exp} attained via OFR369-i(iPrONO). Model simulations revealed that this effect was most pronounced near the reactor inlet (e.g. at low residence time), where the local OH concentration was higher than elsewhere in the reactor because NO_x was very low, resulting in higher sensitivity of [OH] to the OH reactivity of the specific organic nitrite that was used. On the other hand, OFR369-i(1,3-Pr$(ONO)_2$) was less efficient than OFR369-i(iPrONO). In this case, it is possible that higher NO_2 production during 1,3-Pr$(ONO)_2$ photolysis and/or production of more reactive intermediates (e.g. malonaldehyde) offset any benefit gained from faster OH production via photolysis of both -ONO groups or more efficient photolysis of one -ONO group (Wang and Zu, 2016).

3.2.1 ~~Methyl nitrite (MeONO)~~

~~MeONO is commonly used as an OH radical source in environmental chamber studies (Atkinson et al., 1981; Matsunaga and Ziemann, 201 To evaluate its potential use in OFRs, we examined previous measurements in an environmental chamber equipped with blacklights (j_{NO_2} = 0.27 min^{-1}, assumed 350 nm wavelength), where photolysis of 10 ppm MeONO generated OH~2×10^8 molecules cm^{-3} for a few minutes (Atkinson et al., 1981). In our OFR, $j_{NO_2,max}$ = 0.36 min^{-1} at λ = 350 nm. Thus, over 98 sec exposure time, we anticipate $OH_{exp} \approx 2\times10^{10}$ molecules cm^{-3} s would be obtained via photolysis of 10 ppm MeONO in OFRs. This is lower than the OH_{exp} attained via photolysis of 10 ppm iPrONO even after correcting for different j_{NO_2} values in the different studies. Lower OH_{exp} achieved from MeONO photolysis is presumably due to the higher reactivity of formaldehyde, the primary photolysis product of MeONO, relative to acetone, the primary photolysis product of iPrONO at 369 nm(Raff and Finlayson-Pitts, 2010). Along with less efficient OH production, MeONO must be synthesized, trapped at low temperature, and stored under vacuum. Thus, there is no clear advantage to using OFR350-iMeONO (or OFR350-MeONO-d_4) in OFRs relative to OFR369-i(iPrONO) or OFR369-i(iPrONO-d_7).~~

3.2.1 ~~Hexafluoroisopropyl nitrite (HFiPrONO)~~

~~HFiPrONO has been synthesized from O-nitrosation of hexafluoroisopropanol (Andersen et al., 2003; Shuping et al., 2006). We hypothesize that OFR369-i(HFiPrONO) should attain higher OH_{exp} than OFR369-i(iPrONO) and OFR369-i(iPrONO-d_7) due to similar photolysis rates (Andersen et al., 2003) and ~200 times lower OH reactivity of HFiPrONO/hexafluoroacetone relative to iPrONO/acetone (Atkinson et al., 1992; Tokuhashi et al., 1999). We made several unsuccessful attempts to synthesize HFiPrONO and other fluorinated alkyl nitrites with a procedure similar to that used by Andersen et al. (2003) and Shuping et al. (2006). The synthesis product was blue (not yellow) in color when trapped or stored in nitrogen, generated negligible OH upon irradiation in the reactor, and evolved into brown vapor in the presence of air or upon warming to room temperature (Figure S8). These observations suggest the formation of , which we hypothesize was formed in solution from the reactions~~

~~$H_2SO_4 + 2\ NaNO_2 \rightarrow 2HONO + Na_2(SO_4)$ $2HONO \rightarrow NO + NO_2 + H_2O$ $NO + NO_2 \rightleftharpoons N_2O_3$~~

~~This pathway may have been favored if the O-nitrosation of hexafluoroisopropanol was slow compared to non-fluorinated alcohols.~~

3.3 OH_{exp} and NO_2 estimation equations for OFR369-i(iPrONO) and OFR369-i(iPrONO-d_7)

Previous studies reported empirical OH_{exp} algebraic estimation equations for OFR185 and OFR254 (Li et al., 2015; Peng et al., 2015)~~to aid~~ .These equations parameterize OH_{exp} as a function of readily-measured experimental parameters, therefore providing a simpler alternative to detailed photohemical models that aids in experimental planning and analysis. Here, we expand on those studies by deriving OH_{exp} and NO_2 estimation equations for OFR369-i(iPrONO) and OFR369-i(iPrONO-d_7). Model results (14641 model runs in total) obtained from the base case of the model (SO_2 as surrogate of external OH reactivity, "OHR_{ext}") were used to derive the following equations that allow estimating the OH exposure for OFR369-i(iPrONO) and OFR369-i(PrONO-d_7):

$$\log(\mathrm{OH_{exp}}) = \log(\mathrm{I_{369}}) - 0.0026728 \star \mathrm{OHR_{ext}} + 0.46017 \star \log([\mathrm{iPrONO}]) + 1.1928 \star \log(\tau) \quad (3)$$

$$+ 0.35317 \star \log([\mathrm{iPrONO}]) \star \log(\mathrm{OHR_{ext}}) - 0.11109 \star \log(\mathrm{OHR_{ext}}) \star \log(\tau) \quad (4)$$

$$- 0.015606 \star \log(\mathrm{I_{369}}) \star \log([\mathrm{iPrONO}]) \star \log(\tau) - 7.6164 \quad (5)$$

$$\log(\mathrm{OH_{exp}}) = 0.85558 \star \log(\mathrm{I_{369}}) - 0.0029546 \star \mathrm{OHR_{ext}} + 0.61837 \star \log([\mathrm{iPrONO\text{-}d_7}]) \quad (6)$$

$$+ 1.2115 \star \log(\tau) + 0.36081 \star \log([\mathrm{iPrONO\text{-}d_7}]) \star \log(\mathrm{OHR_{ext}}) \quad (7)$$

$$- 0.15501 \star \log(\mathrm{OHR_{ext}}) \star \log(\tau) - 0.017061 \star \log(\mathrm{I_{369}}) \star \log([\mathrm{iPrONO\text{-}d_7}]) \star \log(\tau) \quad (8)$$

$$- 5.1541 \quad (9)$$

where $\mathrm{OH_{exp}}$, I_{369}, $\mathrm{OHR_{ext}}$, [iPrONO or iPrONO-$\mathrm{d_7}$], and τ are in units of molecules $\mathrm{cm^{-3}}$ s, photons $\mathrm{cm^{-2}\ s^{-1}}$, $\mathrm{s^{-1}}$, ppm, and s, respectively. Fit coefficients were obtained by fitting Equations 3 and 6 to $\mathrm{OH_{exp}}$ model results over the following range of OFR parameters: ([iPrONO/iPrONO-$\mathrm{d_7}$]; 0.2-20 ppm), I_{369} (1×10^{15} - 2×10^{16} ~~ph~~ photons $\mathrm{cm^{-2}\ sec^{-1}}$), $\mathrm{OHR_{ext}}$ (1-200 $\mathrm{s^{-1}}$), and residence time, τ, between 30 and 200 sec. We explored 11 logarithmically evenly distributed values in these ranges for each parameter, and thus performed simulations for 14641 model cases in total. To determine the functional form of Equations 3 and 6, we used the sum of the logarithms of first-, second- and third-order terms of the four parameters and iteratively removed the terms with very small fit coefficients until further removal of remaining terms significantly worsened the fit quality.

Figures 5a and 5c compare $\mathrm{OH_{exp}}$ estimated from Equations 3 and 6 and calculated from the model described in Sect. 2.4. The mean absolute value of the relative deviation is 29%, indicating that the estimation equations are typically producing results within the inherent model uncertainties. Care should be taken to not use the equations away from the range of which they were derived, as much larger errors are possible when extrapolating.

While several techniques are available to monitor $\mathrm{NO_2}$, interferences from other nitrogen-containing species are well known and may create issues similar to those shown in Figure 2f. ~~NO2~~ $\mathrm{NO_2}$ production and loss rates are primarily governed by the alkyl nitrite concentration, actinic flux, and residence time in the OFR. These parameters were experimentally constrained (Section 2.2.2). Thus, we derived $\mathrm{NO_2}$ estimation equations for OFR369-i(iPrONO) (Eq. 10) and OFR369-i(iPrONO-$\mathrm{d_7}$) (Eq. 11) as a function of [RONO], I_{369}, and τ, to all of which $\mathrm{NO_2}$ production is proportional, over the same phase space used to ~~derive~~ fit Equations 3 and 6:

$$\log(\mathrm{NO_2}) = \log(\mathrm{I_{369}}) + \log([\mathrm{iPrONO}]) + \log(\tau) - 6.2198 \quad (10)$$

$$\log(\mathrm{NO_2}) = \log(\mathrm{I_{369}}) + \log([\mathrm{iPrONO\text{-}d_7}]) + \log(\tau) - 6.2607 \quad (11)$$

Figures 5b and 5d compare NO_2 estimated from Equations 3 and 6 and calculated from the model described in Sect. 2.4. The mean absolute value of the relative deviation between NO_2 estimated by Equations 10 and 11 and NO_2 computed by the photochemical model is 19%. The mean model NO:NO_2 fraction is approximately 0.33 (Figures 2-3).

3.4 NO_3^--CIMS spectra of organic nitrates generated from α-pinene + OH/OD reactions via OFR369-i(iPrONO), OFR369-i(iPrONO-d_7), and OFR254-iN_2O

To evaluate the efficacy of OFR369-i(iPrONO), OFR369-i(iPrONO-d_7), and OFR254-iN_2O ~~(Lambe et al., 2017; Peng et al., 2018)~~ for generating HO_x under high-NO_x photooxidation conditions, we obtained NO_3^--CIMS spectra of α-pinene + OH/OD nitrogen-containing oxidation products generated using each method~~.~~, with experimental conditions described in Sect. 2.3. ~~In these experiments, the reactor was operated with a residence time of approximately 80 sec to accommodate the undiluted -CIMS inlet flow requirement (10.5 L min^{-1}).~~ Calculated OH exposures for OFR369-i(iPrONO)~~and~~ , OFR369-i(iPrONO-d_7)~~were operated using I_{369} = 6.5×10^{15} photons cm^{-2} s^{-1} and >7 ppm nitrite~~, and OFR254-iN_2O ~~was operated using I_{254} = 3.2×10^{15} photons cm^{-2} s^{-1} + 5 ppm + 1% + 3.2% . Corresponding estimated OH exposures~~ were 2.9×10^{10}, 5.9×10^{10} and ~~4.7~~5.0×10^{11} molecules cm^{-3} s, respectively~~.~~, in the absence of OH consumption due to α-pinene. These calculated steady-state OH_{exp} values decreased to 8.5×10^8, 6.8×10^8 and 4.6×10^{11} molecules cm^{-3} s after accounting for OH consumption. This suggests that most of the OH that was produced in these OFR369-i(iPrONO/iPrONO-d_7) experiments was consumed by α-pinene and its early-generation photooxidation products. OH suppression relative to 254 nm photons, O_3, and O is not a concern in OFR369-i(iPrONO), unlike in OFR254-iN_2O (Peng et al., 2016).

Exposure of α-pinene to OH/OD generated via OFR369-iPrONO, OFR369-iPrONO-d_7, and OFR254-iN_2O produced C_7 - C_{10} organic nitrate and C_{10} dinitrate signals that are shown in Figures 6~~a-c~~ a-d. ($[(NO_3)C_7H_9NO_8]^-$ and $[(NO_3)C_7H_{11}NO_8]^-$ signals at *m/z* = 297 and 299 are excluded due to significant intra- and inter-experiment variability for unknown reasons). Figure 6 shows that many of the same products are observed independent of radical precursor. The Figure 6a spectrum (OFR369-i(iPrONO)) is shifted to lower oxygen-to-carbon ratio relative to ~~Figure 6b~~ Figures 6b (OFR254-iN_2O) and Figure 6c (OFR369-i(iPrONO-d_7)) , consistent with the lower OH_{exp} achieved with OFR369-i(iPrONO) compared to OFR369-i(iPrONO-d_7) and OFR254-iN_2O. For example, $[(NO_3)C_{10}H_{15}NO_7]^-$ was the largest C_{10} nitrate signal observed via OFR369-i(iPrONO), whereas $[(NO_3)C_{10}H_{15}NO_8]^-$ was the largest C_{10} nitrate signal observed via OFR369-i(iPrONO-d_7) and OFR254-iN_2O. Qualitatively similar trends were observed for C_7 - C_9 organic nitrates and C_{10} dinitrates across the three systems.

Two additional features are of note in Figure 6. First, a series of ion signals at *m/z* = 312, 328, 344, 360, 376, 392, 408 and 340, 356, 372, 388, 402, 420 were observed at higher levels ~~in Figure 6b (~~via OFR369-i(iPrONO-d_7) ~~) than~~ relative to OFR369-i(iPrONO). These ions are plotted separately in Figure 6~~a or Figure 6c~~d. The most plausible explanation is the additional contribution of $[(NO_3)C_8H_{10}DNO_{8-14}]^-$ and $[(NO_3)C_{10}H_{14}DNO_{7-14}]^-$ ions that retain -OD functionality following initial addition of OD (rather than OH) to α-pinene. There is evidence of other deuterium-containing ions in Figure 6b that are either less prominent or more difficult to resolve from other ions at the same integer mass. Second, C_{10} dinitrates were present in all three spectra, with the highest dinitrate ~~:nitrate ratios~~ fractions observed in Figures 6b (0.090) and 6c (0.081), and the lowest dinitrate fraction observed in Figure 6a (0.056). Dinitrates are presumably generated from α-pinene following

(1) two OH reactions followed by two RO_2 + NO termination reactions or (2) one NO_3 reaction followed by one RO_2 + NO termination reaction. Previous application of OFR254-iN_2O could not exclude the contribution of α-pinene + NO_3 reactions, with NO_3 radicals generated from NO_2 + O_3 and other reactions (Lambe et al., 2017). However, generation of dinitrates via OFR369-i(iPrONO-d_7), which produced negligible NO_3, suggests that dinitrates are not an artifact of unwanted α-pinene + NO_3 reactions.

The ability of OFR369-i(iPrONO) and OFR369-i(iPrONO-d_7) to mimic polluted atmospheric conditions can be evaluated by comparing signals observed in ~~Figure 6with published~~ Figures 6a-c with NO_3^--CIMS spectra obtained in Centreville, AL, USA (Massoli et al., 2018) and in Hyytiala, Finland (Yan et al., 2016) that are shown in Figures 6e-f. Both measurement locations are influenced by local biogenic emissions mixed with occasional anthropogenic outflow. Figures 6e and 6f were obtained on 25 June 2013 (7:30–11:00 Centreville time) and 11 April 2012 (10:00-13:00 Hyytiala time) respectively. The mean NO mixing ratios during these periods were 0.53±0.17 (Centreville) and 0.27±0.09 ppb (Hyytiala). In Centreville, a "terpene nitrate" source factor that peaked during the early morning contained $C_9H_{15}NO_{5-7}$, $C_{10}H_{15,17}NO_{6-10}$, and $C_{10}H_{14,16}N_2O_{8-11}$ compounds (Massoli et al., 2018). The largest C_{10} nitrate and dinitrate species in that factor were $C_{10}H_{15}NO_6$, $C_{10}H_{15}NO_8$, $C_{10}H_{16}N_2O_9$ and $C_{10}H_{16}N_2O_{10}$. In Hyytiala, ~~a factor that~~ concentrations of $C_{10}H_{15}NO_{7-11}$ and $C_{10}H_{16}N_2O_{8-11}$ peaked in the ~~early morning had significant and contributions, and a separate factor that peaked in the afternoonwas dominated by (Yan et al., 2016). Figure 6 indicates that all of these compounds~~ morning and early afternoon. Elevated C_{10} dinitrate levels during the daytime in Hyytiaila (Figure 6f suggest their formation from monoterpenes following two OH reactions followed by two RO_2 + NO termination reactions, as proposed earlier.

Overall, Figure 6 shows that many of the C7-C10 nitrogen-containing compounds observed in Centreville and Hyytiala were generated via OFR369-i(iPrONO), OFR369-i(iPrONO-d_7) and OFR254-iN_2O. ~~Overall, due~~ Due to the local nature of the ambient terpene emissions at the Centreville and Hyytiala sites, the associated photochemical age was presumably ~~<~~<1 day. Thus, while the ambient NO_3^--CIMS spectra at those sites were more complex and contained contributions from precursors other than α-pinene, the oxidation state of the ambient terpene-derived organic nitrates was more closely simulated via OFR369-i(iPrONO) or OFR369-i(iPrONO-d_7), where the largest C_{10} nitrates and dinitrates were $C_{10}H_{15}NO_7$ and $C_{10}H_{16}N_2O_9$ (OFR369-i(iPrONO); Figure 6a), and $C_{10}H_{15}NO_8$, $C_{10}H_{15}NO_9$ and $C_{10}H_{16}N_2O_9$ (OFR369-i(iPrONO-d_7); Figure 6~~b~~c). By comparison, $C_{10}H_{15}NO_8$ and $C_{10}H_{16}N_2O_{11}$ were the largest nitrate and dinitrate species generated via OFR254-iN_2O (Figure 6~~e~~b).

3.5 Anticipated performance of alternative high-NO_x HO_x precursors in OFRs

3.5.1 Methyl nitrite (MeONO)

MeONO is commonly used as an OH radical source in environmental chamber studies (Atkinson et al., 1981; Matsunaga and Ziemann, 201 To evaluate its potential use in OFRs, we examined previous measurements in an environmental chamber equipped with blacklights (j_{NO_2} = 0.27 min^{-1}, assumed 350 nm wavelength), where photolysis of 10 ppm MeONO generated [OH] ~2×10^8 molecules cm^{-3} for a few minutes (Atkinson et al., 1981). In our OFR, $j_{NO_2,max}$ = 0.36 min^{-1} at λ = 350 nm. Thus, over 98

sec exposure time, we anticipate $OH_{exp} \approx 2\times10^{10}$ molecules cm^{-3} s would be obtained via photolysis of 10 ppm MeONO in OFRs. This is lower than the OH_{exp} attained via photolysis of 10 ppm iPrONO even after correcting for different j_{NO_2} values in the different studies. Lower OH_{exp} achieved from MeONO photolysis is presumably due to the higher reactivity of formaldehyde, the primary photolysis product of MeONO, relative to acetone, the primary photolysis product of iPrONO at 369 nm (Raff and Finlayson-Pitts, 2010). Along with less efficient OH production, MeONO must be synthesized, trapped at low temperature, and stored under vacuum. Thus, there is no advantage to using OFR350-iMeONO (or OFR350-MeONO-d_4) in OFRs relative to OFR369-i(iPrONO) or OFR369-i(iPrONO-d_7).

3.5.2 Nitrous acid (HONO)

HONO is also commonly used as an OH radical source in environmental chamber studies. To evaluate its potential application in OFRs, we examined previous measurements in an environmental chamber equipped with blacklights, where photolysis of 3-20 ppm HONO generated initial [OH] $\approx 6\times10^7$ molecules cm^{-3} (Cox et al., 1980), which is 3.3 times lower than [OH] obtained from photolysis of comparable levels of MeONO (Section 3.5.1). Lower OH_{exp} achieved from HONO photolysis is presumably due to higher OH reactivity of HONO relative to MeONO/iPrONO. Additionally, HONO is difficult to prepare without NO_2 impurities (Febo et al., 1995) that may cause additional OH suppression. For these reasons, we believe that there is no advantage to using HONO as a HO_x precursor in OFRs.

3.5.3 Hexafluoroisopropyl nitrite (HFiPrONO)

HFiPrONO has been synthesized from O-nitrosation of hexafluoroisopropanol (Andersen et al., 2003; Shuping et al., 2006). We predict that OFR369-i(HFiPrONO) should attain higher OH_{exp} than OFR369-i(iPrONO) and OFR369-i(iPrONO-d_7) due to similar photolysis rates (Andersen et al., 2003) and ~200 times lower OH reactivity of HFiPrONO/hexafluoroacetone relative to iPrONO/acetone (Atkinson et al., 1992; Tokuhashi et al., 1999). Simple modeling calculations suggest that application of OFR369-i(HFiPrONO) may achieve up to a week of equivalent OH exposure. We made several unsuccessful attempts to synthesize HFiPrONO and other fluorinated alkyl nitrites with a procedure similar to that used by Andersen et al. (2003) and Shuping et al. (2006). The synthesis product was blue (not yellow) in color when trapped or stored in nitrogen, generated negligible OH upon irradiation in the reactor, and evolved into brown vapor in the presence of air or upon warming to room temperature (Figure S8). These observations suggest the formation of N_2O_3, which we hypothesize was formed in solution from the reactions

$$H_2SO_4 + 2NaNO_2 \rightarrow 2HONO + Na_2(SO_4) \quad \text{(R18)}$$

$$2HONO \rightarrow NO + NO_2 + H_2O \quad \text{(R19)}$$

$$NO + NO_2 \rightleftharpoons N_2O_3 \quad \text{(R20)}$$

This pathway may have been favored if the O-nitrosation of hexafluoroisopropanol was slow compared to non-fluorinated alcohols.

4 Conclusions

Recently, we developed new methods that enable NO_x-dependent photooxidation studies in OFRs using $O(^1D) + N_2O + H_2O$ reactions via O_3 photolysis at λ = 254 nm and/or $H_2O + N_2O$ photolysis at 185 nm (OFR254-iN_2O and OFR185-iN_2O) (Lambe et al., 2017; Peng et al., 2018). Alkyl nitrite photolysis is an established method that facilitates high-NO_x photooxidation studies in modern OFRs. Here, we adapted alkyl nitrite photolysis for new OFR applications by characterizing the photolysis wavelength, nitrite concentration, and nitrite composition that result in optimal HO_x and NO_x generation capabilities. Based on our results, we recommend photolysis of 5-10 ppm isopropyl nitrite at $\lambda \approx$ 365 - 370 nm photolysis wavelength and $I > 10^{15}$ photons cm^{-2} s^{-1}. If the user has the resources to synthesize iPrONO-d_7, better performance is expected relative to iPrONO. Alkyl nitrite photolysis at λ = 254 nm is not recommended. Taken together, OFR254/185-iN_2O and OFR369-i(iPrONO/iPrONO-d_7) ~~methods~~ are complementary methods that provide additional flexibility for NO_x-dependent OFR studies. OFR254/OFR185-iN_2O and OFR185-iN_2O generate variable-NO_x photooxidation conditions (NO:$HO_2 \approx$ 0 - 100) and are suitable for to the characterization of multigenerational oxidative aging processes at up to $OH_{exp} \approx (5\text{-}10)\times10^{11}$ molecules cm^{-3} s ($\sim$ 5-10 equivalent days). OFR369-i(iPrONO)/OFR369-i(iPrONO-d_7) generate high-NO ~~$_x$~~ photooxidation conditions (NO:$HO_2 \approx$ 10 - 10000; NO:$NO_2 \approx$ 0.2-0.7) with minimal O_3 and NO_3 formation at longer photolysis wavelength than OFR254/185-iN_2O. We anticipate that alkyl nitrite photolysis is ~~suitable~~ advantageous for the characterization of first-generation, high-NO_x photooxidation products of most precursors at up to $OH_{exp} \approx 1\times10^{11}$ molecules cm^{-3} s (1 equivalent day), which is comparable to environmental chambers investigating high-NO_x conditions. The generation of OD (rather than OH) via OFR369-i(iPrONO-d_7) may be useful in photooxidation studies of unsaturated precursors due to the shift on the *m/z* of the addition products, though at the potential expense of generating more complex distributions of oxidation products. ~~OFR254-iN_2O and OFR185-iN_2O generate variable-photooxidation conditions (NO: $\approx$ 0 - 100) (Lambe et al., 2017; Peng et al., 2018), and, due to higher attainable~~ Potential disadvantages of the OFR369-i(iPrONO) method are: (1) restriction to high-NO photochemical conditions; (2) restriction to OH_{exp} ~~, are potentially better suited to the characterization of multigenerational oxidative aging processes~~of 1 equivalent day or less; (3) additional complexity involved with integration of the alkyl nitrite source (compared to O_3 + H_2O + N_2O); (4) additional cost and complexity to retrofit a specific OFR design with blacklights; (5) it acts as an interference that precludes NOx measurements by chemiluminescence detection. Future work will evaluate the ability of each method to mimic polluted atmospheric conditions in specific source regions.

Data availability. Data presented in this manuscript is available upon request.

Competing interests. The authors declare no competing interests.

Acknowledgements. This research was supported by the Atmospheric Chemistry Program of the US National Science Foundation under grants AGS-1536939, AGS-1537446, AGS-1537009, and AGS-1352375 (to JDR). ZP and JLJ were supported by DOE (BER/ASR) DE-SC0016559 and NOAA NA18OAR4310113. ATL thanks Paola Massoli, Penglin Ye, and Phil Croteau (ARI) for experimental assistance, and Chao Yan (University of Helsinki), William Brune (Penn State), Pengfei Liu (Harvard), Wai Yip Fan (National University of Singapore), Manjula Canagaratna (ARI), John Jayne (ARI), Charles Kolb (ARI), and Paul Ziemann (CU Boulder) for helpful discussions.

References

Andersen, M. P. S., Hurley, M. D., Ball, J. C., Schneider, W. F., Wallington, T. J., and Nielsen, O. J.: $CF_3CH(ONO)CF_3$: Synthesis, IR spectrum, and use as OH radical source for kinetic and mechanistic studies, International Journal of Chemical Kinetics, 35, 159–165, https://doi.org/10.1002/kin.10116, http://dx.doi.org/10.1002/kin.10116, 2003.

Atkinson, R., Carter, W. P. L., Winer, A. M., and Jr., J. N. P.: An Experimental Protocol for the Determination of OH Radical Rate Constants with Organics Using Methyl Nitrite Photolysis as an OH Radical Source, Journal of the Air Pollution Control Association, 31, 1090–1092, https://doi.org/10.1080/00022470.1981.10465331, https://doi.org/10.1080/00022470.1981.10465331, 1981.

Atkinson, R., Baulch, D., Cox, R., Hampson, R., Kerr, J., and Troe, J.: Evaluated kinetic and photochemical data for atmospheric chemistry: Supplement IV: IUPAC subcommittee on gas kinetic data evaluation for atmospheric chemistry, Atmospheric Environment. Part A. General Topics, 26, 1187 – 1230, https://doi.org/https://doi.org/10.1016/0960-1686(92)90383-V, http://www.sciencedirect.com/science/article/pii/096016869290383V, 1992.

Atkinson, R., Baulch, D. L., Cox, R. A., Crowley, J. N., Hampson, R. F., Hynes, R. G., Jenkin, M. E., Rossi, M. J., and Troe, J.: Evaluated kinetic and photochemical data for atmospheric chemistry: Volume I - gas phase reactions of O_x, HO_x, NO_x and SO_x species, Atmospheric Chemistry and Physics, 4, 1461–1738, https://doi.org/10.5194/acp-4-1461-2004, https://www.atmos-chem-phys.net/4/1461/2004/, 2004.

Bertram, T. H., Kimmel, J. R., Crisp, T. A., Ryder, O. S., Yatavelli, R. L. N., Thornton, J. A., Cubison, M. J., Gonin, M., and Worsnop, D. R.: A field-deployable, chemical ionization time-of-flight mass spectrometer, Atmospheric Measurement Techniques, 4, 1471–1479, 2011.

BIPM, IEC, IFCC, ILAC, ISO, IUPAC, and 101, I. J.: Evaluation of measurement data - Supplement 1 to the "Guide to the expression of uncertainty in measurement" - Propagation of distributions using a Monte-Carlo method, http://www.bipm.org/utils/common/documents/jcgm/JCGM_101_2008_E.pdf, last access: December 2016, 2008.

Burkholder, J. B., Sander, S. P., Abbatt, J. P. D., Barker, J. R., Huie, R. E., Kolb, C. E., Kurylo, M. J., L., O. V., Wilmouth, D. M., , and Wine, P. H.: Chemical Kinetics and Photochemical Data for Use in Atmospheric Studies, Evaluation Number 18, Pasadena, CA, USA,, http://jpldataeval.jpl.nasa.gov/, last access: February 2017, 2015.

Calvert, J. G. and Pitts, J. N.: Photochemistry, John Wiley & Sons, Inc.: New York, NY, 1966.

Carrasquillo, A. J., Hunter, J. F., Daumit, K. E., and Kroll, J. H.: Secondary Organic Aerosol Formation via the Isolation of Individual Reactive Intermediates: Role of Alkoxy Radical Structure, The Journal of Physical Chemistry A, 118, 8807–8816, https://doi.org/10.1021/jp506562r, http://dx.doi.org/10.1021/jp506562r, pMID: 25148415, 2014.

Chhabra, P., Ng, N., Canagaratna, M., Corrigan, A., Russell, L., Worsnop, D., Flagan, R., and Seinfeld, J.: Elemental composition and oxidation of chamber organic aerosol, Atmospheric Chemistry and Physics, 11, 8827–8845, 2011.

Cox, R. A., Derwent, R. G., and Williams, M. R.: Atmospheric photooxidation reactions. Rates, reactivity, and mechanism for reaction of organic compounds with hydroxyl radicals, Environmental Science & Technology, 14, 57–61, https://doi.org/10.1021/es60161a007, http://dx.doi.org/10.1021/es60161a007, pMID: 22229993, 1980.

Ehn, M., Kleist, E., Junninen, H., Petäjä, T., Lönn, G., Schobesberger, S., Dal Maso, M., Trimborn, A., Kulmala, M., Worsnop, D. R., Wahner, A., Wildt, J., and Mentel, T. F.: Gas phase formation of extremely oxidized pinene reaction products in chamber and ambient air, Atmospheric Chemistry and Physics, 12, 5113–5127, 2012.

Ehn, M., Thornton, J. A., Kleist, E., Sipilä, M., Junninen, H., Pullinen, I., Springer, M., Rubach, F., Tillmann, R., Lee, B., Lopez-Hilfiker, F., Andres, S., Acir, I.-H., Rissanen, M., Jokinen, T., Schobesberger, S., Kangasluoma, J., Kontkanen, J., Nieminen, T., Kurten, T., Nielsen,

L. B., Jørgensen, S., Kjaergaard, H. G., Canagaratna, M., Maso, M. D., Berndt, T., Petäjä, T., Wahner, A., Kerminen, V.-M., Kulmala, M., Worsnop, D. R., Wildt, J., and Mentel, T. F.: A large source of low-volatility secondary organic aerosol, Nature, 506, 476–479, 2014.

Eisele, F. L. and Tanner, D. J.: Measurement of the gas phase concentration of H_2SO_4 and methane sulfonic acid and estimates of H_2SO_4 production and loss in the atmosphere, Journal of Geophysical Research: Atmospheres, 98, 9001–9010, https://doi.org/10.1029/93JD00031, http://dx.doi.org/10.1029/93JD00031, 1993.

Febo, A., Perrino, C., Gherardi, M., and Sparapani, R.: Evaluation of a high-purity and high-stability continuous generation system for nitrous acid, Environmental Science and Technology, 29, 2390–2395, 1995.

Finewax, Z., de Gouw, J. A., and Ziemann, P. J.: Identification and Quantification of 4-Nitrocatechol Formed from OH and NO3 Radical-Initiated Reactions of Catechol in Air in the Presence of NOx: Implications for Secondary Organic Aerosol Formation from Biomass Burning, Environmental Science & Technology, 52, 1981–1989, https://doi.org/10.1021/acs.est.7b05864, https://doi.org/10.1021/acs.est.7b05864, pMID: 29353485, 2018.

Gardner, E. P., Sperry, P. D., and Calvert, J. G.: Primary quantum yields of NO_2 photodissociation, Journal of Geophysical Research: Atmospheres, 92, 6642–6652, https://doi.org/10.1029/JD092iD06p06642, http://dx.doi.org/10.1029/JD092iD06p06642, 1987.

Huang, Y., Coggon, M. M., Zhao, R., Lignell, H., Bauer, M. U., Flagan, R. C., and Seinfeld, J. H.: The Caltech Photooxidation Flow Tube reactor: design, fluid dynamics and characterization, Atmospheric Measurement Techniques, 10, 839–867, https://doi.org/10.5194/amt-10-839-2017, https://www.atmos-meas-tech.net/10/839/2017/, 2017.

Krechmer, J. E., Coggon, M. M., Massoli, P., Nguyen, T. B., Crounse, J. D., Hu, W., Day, D. A., Tyndall, G. S., Henze, D. K., Rivera-Rios, J. C., Nowak, J. B., Kimmel, J. R., Mauldin, III, R. L., Stark, H., Jayne, J. T., Sipilä, M., Junninen, H., Clair, J. M. S., Zhang, X., Feiner, P. A., Zhang, L., Miller, D. O., Brune, W. H., Keutsch, F. N., Wennberg, P. O., Seinfeld, J. H., Worsnop, D. R., Jimenez, J. L., and Canagaratna, M. R.: Formation of Low Volatility Organic Compounds and Secondary Organic Aerosol from Isoprene Hydroxyhydroperoxide Low-NO Oxidation, Environmental Science and Technology, 49, 10 330–10 339, 2015.

Lambe, A. T., Ahern, A. T., Williams, L. R., Slowik, J. G., Wong, J. P. S., Abbatt, J. P. D., Brune, W. H., Ng, N. L., Wright, J. P., Croasdale, D. R., Worsnop, D. R., Davidovits, P., and Onasch, T. B.: Characterization of aerosol photooxidation flow reactors: heterogeneous oxidation, secondary organic aerosol formation and cloud condensation nuclei activity measurements, Atmospheric Measurement Techniques, 4, 445–461, 2011.

Lambe, A. T., Onasch, T. B., Croasdale, D. R., Wright, J. P., Martin, A. T., Franklin, J. P., Massoli, P., Kroll, J. H., Canagaratna, M. R., Brune, W. H., Worsnop, D. R., and Davidovits, P.: Transitions from Functionalization to Fragmentation Reactions of Laboratory Secondary Organic Aerosol (SOA) Generated from the OH Oxidation of Alkane Precursors, Environmental Science and Technology, 46, 5430–5437, 2012.

Lambe, A. T., Massoli, P., Zhang, X., Canagaratna, M. R., Nowak, J. B., Daube, C., Yan, C., Nie, W., Onasch, T. B., Jayne, J. T., Kolb, C. E., Davidovits, P., Worsnop, D. R., and Brune, W. H.: Controlled nitric oxide production via $O(^1D) + N_2O$ reactions for use in oxidation flow reactor studies, Atmospheric Measurement Techniques, 10, 2283–2298, https://doi.org/10.5194/amt-10-2283-2017, https://www.atmos-meas-tech.net/10/2283/2017/, 2017.

Lee, J. D., Whalley, L. K., Heard, D. E., Stone, D., Dunmore, R. E., Hamilton, J. F., Young, D. E., Allan, J. D., Laufs, S., and Kleffmann, J.: Detailed budget analysis of HONO in central London reveals a missing daytime source, Atmospheric Chemistry and Physics, 16, 2747–2764, https://doi.org/10.5194/acp-16-2747-2016, https://www.atmos-chem-phys.net/16/2747/2016/, 2016.

Li, R., Palm, B. B., Ortega, A. M., Hlywiak, J., Hu, W., Peng, Z., Day, D. A., Knote, C., Brune, W. H., De Gouw, J. A., and Jimenez, J. L.: Modeling the Radical Chemistry in an Oxidation Flow Reactor: Radical Formation and Recycling, Sensitivities, and the OH Exposure Estimation Equation, The Journal of Physical Chemistry A, 119, 150406123535 006, 2015.

Liu, P. F., Abdelmalki, N., Hung, H.-M., Wang, Y., Brune, W. H., and Martin, S. T.: Ultraviolet and visible complex refractive indices of secondary organic material produced by photooxidation of the aromatic compounds toluene and *m*-xylene, Atmospheric Chemistry and Physics, 15, 1435–1446, 2015.

Mao, J., Ren, X., Brune, W., Olson, J., Crawford, J., Fried, A., Huey, L., Cohen, R., Heikes, B., and Singh, H.: Airborne measurement of OH reactivity during INTEX-B, Atmospheric Chemistry and Physics, 9, 163–173, 2009.

Massoli, P., Stark, H., Canagaratna, M. R., Krechmer, J. E., Xu, L., Ng, N. L., Mauldin, R. L., Yan, C., Kimmel, J. R., Misztal, P. K., Jimenez, J. L., Jayne, J. T., and Worsnop, D. R.: Ambient Measurements of Highly Oxidized Gas Phase Molecules during the Southern Oxidant and Aerosol Study (SOAS) 2013, ACS Earth and Space Chemistry, 2, 653–672, https://doi.org/10.1021/acsearthspacechem.8b00028, https://doi.org/10.1021/acsearthspacechem.8b00028, 2018.

Matsunaga, A. and Ziemann, P. J.: Yields of -β-hydroxynitrates, dihydroxynitrates, and trihydroxynitrates formed from OH radical-initiated reactions of 2-methyl-1-alkenes, Proceedings of the National Academy of Sciences, 107, 6664–6669, https://doi.org/10.1073/pnas.0910585107, http://www.pnas.org/content/107/15/6664, 2010.

Ng, N. L., Herndon, S. C., Trimborn, A., Canagaratna, M. R., Croteau, P. L., Onasch, T. B., Sueper, D., Worsnop, D. R., Zhang, Q., Sun, Y. L., and Jayne, J. T.: An Aerosol Chemical Speciation Monitor (ACSM) for Routine Monitoring of the Composition and Mass Concentrations of Ambient Aerosol, Aerosol Science and Technology, 45, 770–784, 2011.

Nielsen, O. J., Sidebottom, H. W., O'Farrell, D. J., Donlon, M., and Treacy, J.: Absolute and relative rate constants for the gas-phase reaction of OH radicals with CH_3NO_2, CD_3NO_2 and $CH_3CH_2CH_3$ at 295 K and 1 atm, Chemical Physics Letters, 146, 197 – 203, https://doi.org/https://doi.org/10.1016/0009-2614(88)87430-X, http://www.sciencedirect.com/science/article/pii/000926148887430X, 1988.

Nielsen, O. J., Sidebottom, H. W., Donlon, M., and Treacy, J.: Rate constants for the gas-phase reactions of OH radicals and Cl atoms with n-alkyl nitrites at atmospheric pressure and 298 K, International Journal of Chemical Kinetics, 23, 1095–1109, https://doi.org/10.1002/kin.550231204, http://dx.doi.org/10.1002/kin.550231204, 1991.

Noyes, W. A.: Explanation of the Formation of Alkyl Nitrites in Dilute Solutions; Butyl and Amyl Nitrites, Journal of the American Chemical Society, 55, 3888–3889, https://doi.org/10.1021/ja01336a503, http://dx.doi.org/10.1021/ja01336a503, 1933.

Orlando, J. J. and Tyndall, G. S.: Laboratory studies of organic peroxy radical chemistry: an overview with emphasis on recent issues of atmospheric significance, Chem. Soc. Rev., 41, 6294–6317, https://doi.org/10.1039/C2CS35166H, http://dx.doi.org/10.1039/C2CS35166H, 2012.

Peng, Z. and Jimenez, J. L.: Modeling of the chemistry in oxidation flow reactors with high initial NO, Atmospheric Chemistry and Physics, 17, 11 991–12 010, https://doi.org/10.5194/acp-17-11991-2017, https://www.atmos-chem-phys.net/17/11991/2017/, 2017.

Peng, Z., Day, D. A., Stark, H., Li, R., Lee-Taylor, J., Palm, B. B., Brune, W. H., and Jimenez, J. L.: HO_x radical chemistry in oxidation flow reactors with low-pressure mercury lamps systematically examined by modeling, Atmospheric Measurement Techniques, 8, 4863–4890, 2015.

Peng, Z., Day, D. A., Ortega, A. M., Palm, B. B., Hu, W., Stark, H., Li, R., Tsigaridis, K., Brune, W. H., and Jimenez, J. L.: Non-OH chemistry in oxidation flow reactors for the study of atmospheric chemistry systematically examined by modeling, Atmospheric Chemistry and Physics, 16, 4283–4305, https://doi.org/10.5194/acp-16-4283-2016, http://www.atmos-chem-phys.net/16/4283/2016/, 2016.

Peng, Z., Palm, B. B., Day, D. A., Talukdar, R. K., Hu, W., Lambe, A. T., Brune, W. H., and Jimenez, J. L.: Model Evaluation of New Techniques for Maintaining High-NO Conditions in Oxidation Flow Reactors for the Study of OH-Initiated Atmospheric Chemistry, ACS Earth and Space Chemistry, 2, 72–86, https://doi.org/10.1021/acsearthspacechem.7b00070, https://doi.org/10.1021/acsearthspacechem.7b00070, 2018.

Raff, J. D. and Finlayson-Pitts, B. J.: Hydroxyl Radical Quantum Yields from Isopropyl Nitrite Photolysis in Air, Environmental Science & Technology, 44, 8150–8155, https://doi.org/10.1021/es102218d, http://dx.doi.org/10.1021/es102218d, pMID: 20879762, 2010.

Raff, J. D., Stevens, P. S., and Hites, R. A.: Relative Rate and Product Studies of the OH-Acetone Reaction, The Journal of Physical Chemistry A, 109, 4728–4735, https://doi.org/10.1021/jp0501547, http://dx.doi.org/10.1021/jp0501547, pMID: 16833814, 2005.

Shuping, L., Chwee, T. S., and Fan, W. Y.: FTIR studies on the gas phase laser-induced decomposition of CF_3CH_2ONO, Chemical Physics, 320, 259 – 266, https://doi.org/https://doi.org/10.1016/j.chemphys.2005.07.020, http://www.sciencedirect.com/science/article/pii/S0301010405003046, 2006.

Tokuhashi, K., Nagai, H., Takahashi, A., Kaise, M., Kondo, S., Sekiya, A., Takahashi, M., Gotoh, Y., and Suga, A.: Measurement of the OH Reaction Rate Constants for CF_3CH_2OH, $CF_3CF_2CH_2OH$, and $CF_3CH(OH)CF_3$, The Journal of Physical Chemistry A, 103, 2664–2672, https://doi.org/10.1021/jp983961x, https://doi.org/10.1021/jp983961x, 1999.

Wang, L. and Zu, L.: Photodissociation dynamics of dinitrite at 355 nm: initiation of a reactive pathway, Phys. Chem. Chem. Phys., 18, 25 249–25 256, https://doi.org/10.1039/C6CP03049A, http://dx.doi.org/10.1039/C6CP03049A, 2016.

Yan, C., Nie, W., Äijälä, M., Rissanen, M. P., Canagaratna, M. R., Massoli, P., Junninen, H., Jokinen, T., Sarnela, N., Häme, S. A. K., Schobesberger, S., Canonaco, F., Yao, L., Prévôt, A. S. H., Petäjä, T., Kulmala, M., Sipilä, M., Worsnop, D. R., and Ehn, M.: Source characterization of highly oxidized multifunctional compounds in a boreal forest environment using positive matrix factorization, Atmospheric Chemistry and Physics, 16, 12 715–12 731, 2016.

Ye, J., Abbatt, J. P. D., and Chan, A. W. H.: Novel pathway of SO_2 oxidation in the atmosphere: reactions with monoterpene ozonolysis intermediates and secondary organic aerosol, Atmospheric Chemistry and Physics, 18, 5549–5565, https://doi.org/10.5194/acp-18-5549-2018, https://www.atmos-chem-phys.net/18/5549/2018/, 2018.

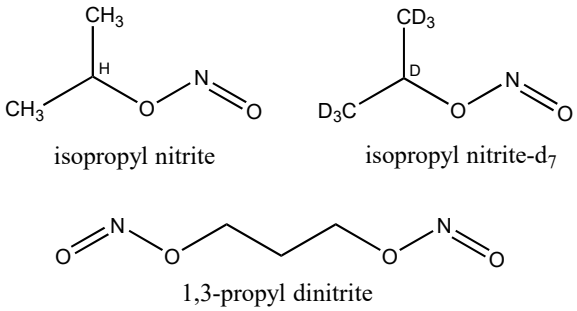

Figure 1. Molecular structures of isopropyl nitrite, isopropyl nitrite-d_7 (d = deuterium = ^{2}H), and 1,3-propyl dinitrite.

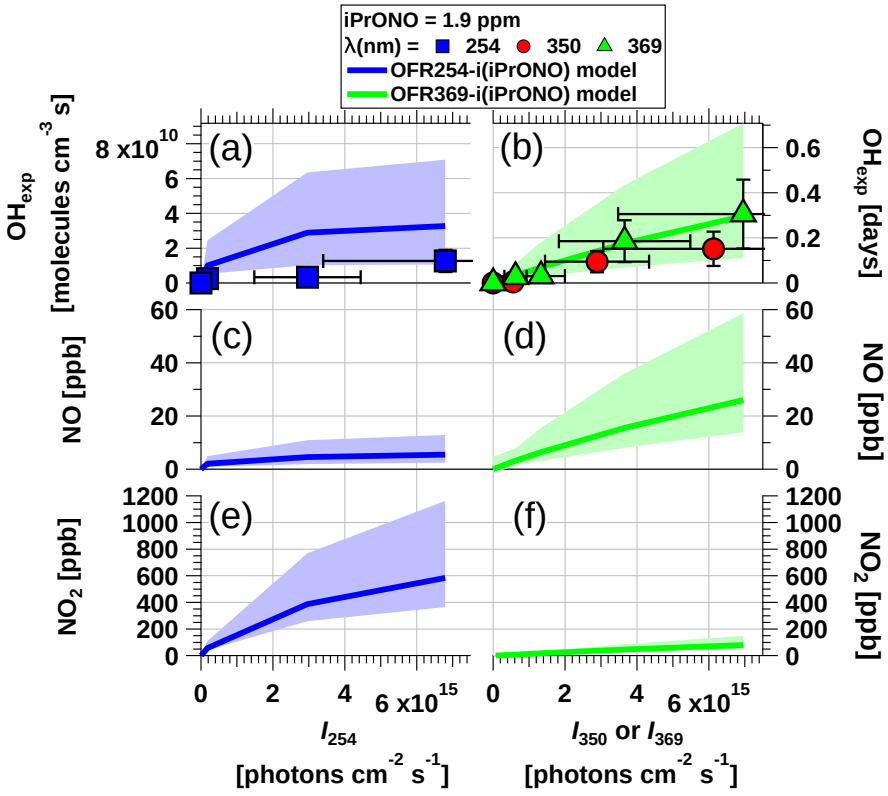

Figure 2. Measured and modeled (a-b) OH exposure, (c-d) NO mixing ratio, and (e-f) NO_2 mixing ratio values as a function of actinic flux (I) following photolysis of 1.9 ppm isopropyl nitrite (iPrONO) at λ = 254 (OFR254-i(iPrONO)), 350, or 369 nm (OFR369-i(iPrONO)) in the PAM oxidation flow reactor. Error bars for measurements represent $\pm$50% uncertainty in OH_{exp} and I-values.

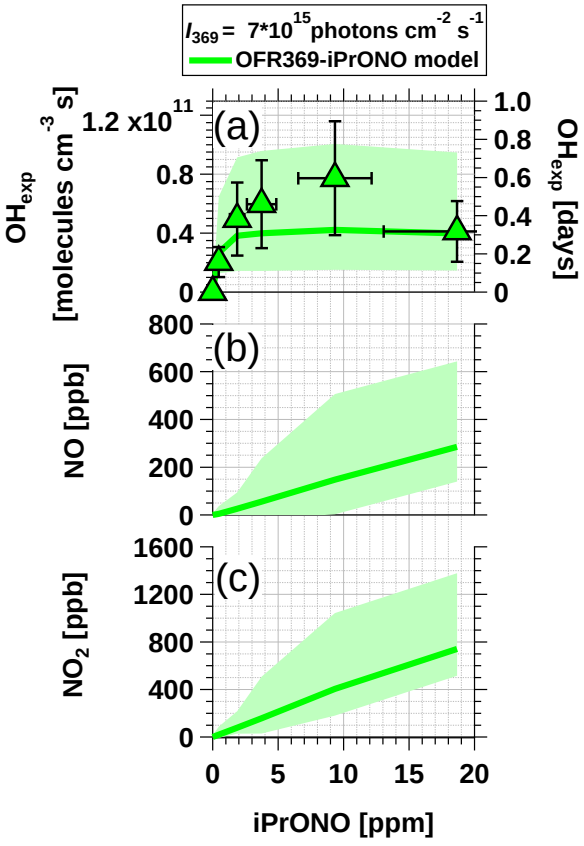

Figure 3. Measured and modeled (a) OH exposure, (b) NO mixing ratio and (c) NO_2 mixing ratio values obtained using OFR369-i(iPrONO) at I_{369} = 7×10^{15} ph cm^{-2} sec^{-1} as a function of iPrONO mixing ratio. Error bars for measurements represent $\pm$50% uncertainty in OH_{exp} and estimated $\pm$30% uncertainty in iPrONO mixing ratio values.

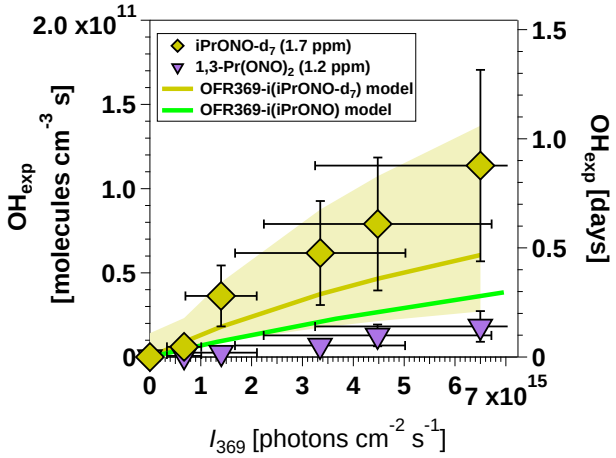

Figure 4. Measured and modeled OH exposure values measured as a function of I_{369} following photolysis of perdeuterated isopropyl nitrite (iPrONO-d_7) and 1,3-propyl dinitrite (1,3-Pr$(ONO)_2$). Modeled OH_{exp} values obtained from OFR369-i(iPrONO-d_7) and OFR369-i(iPrONO) ~~from~~ (Fig. 2d) are shown for reference. Error bars for measurements represent $\pm$50% uncertainty in OH_{exp} and I-values.

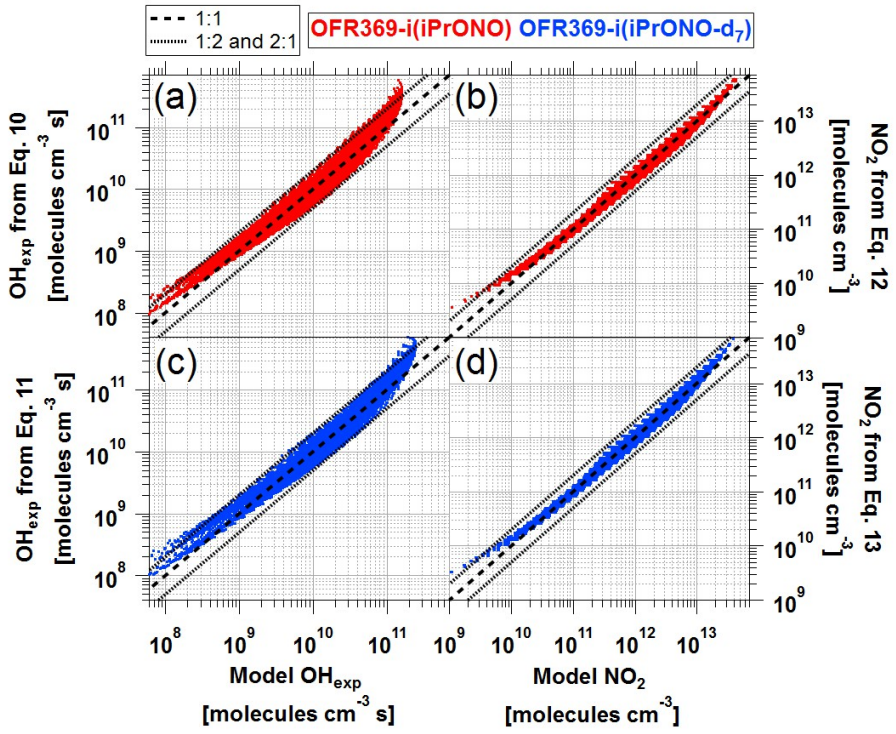

Figure 5. ~~NO_3^--CIMS spectra~~ Comparision of ~~nitrogen-containing α-pinene photooxidation products with~~ OH_{exp} and NO_2 values obtained from estimation equations and photochemical model for (~~“, , ”~~a-b) ~~, (“”), (“D”), (“D”) or (“dinitrate”) formulas generated via (a)~~ OFR369-i(iPrONO) and (bc-d) OFR369-i(iPrONO-d_7) ~~(c) OFR254-i(= 1%, = 3.2%)~~. ~~“” labels indicate number of oxygen atoms in corresponding signals (excluding 3 oxygen atoms per nitrate functional group).~~

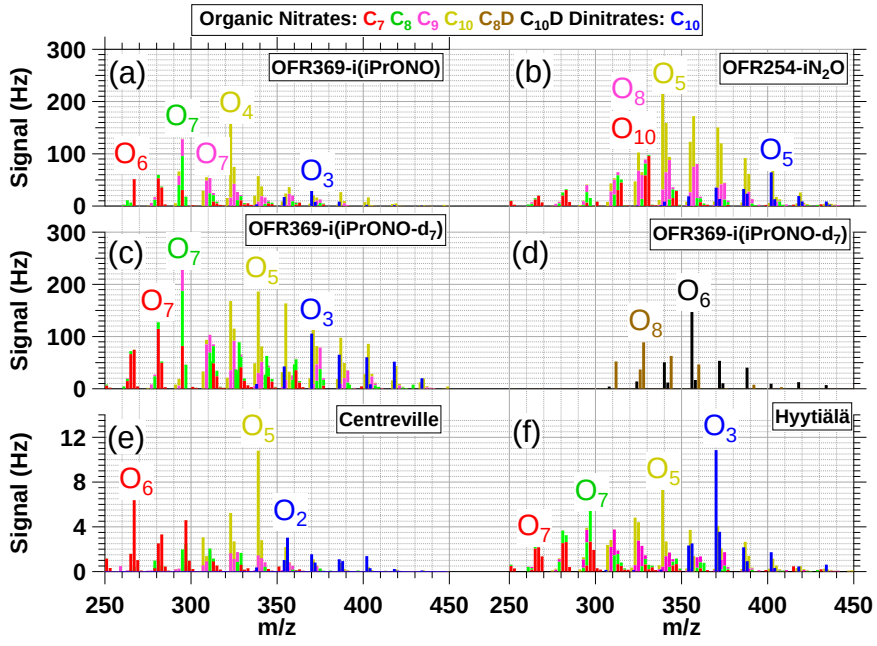

Figure 6. NO_3^--CIMS spectra of nitrogen-containing α-pinene photooxidation products with $C_{7-9}H_{9,11,13,15}NO_{5-10}$ ("C_7, C_8, C_9"), $C_{10}H_{15,17}NO_{4-14}$ ("C_{10}"), $C_8H_{8,10}DNO_{8-14}$ ("C_8D"), $C_{10}H_{14,16}DNO_{7-14}$ ("$C_{10}D$") or $C_{10}H_{16,18}N_2O_{6-13}$ ("C_{10} dinitrate") formulas generated via (a) OFR369-i(iPrONO) (b) OFR254-iN_2O (H_2O = 1%, N_2O = 3.2%). (c,d) OFR369-i(iPrONO-d_7) and observed in ambient measurements at (e) Centreville, Alabama, United States (Massoli et al., 2018) (f) Hyytiala, Finland (Yan et al., 2016). "O_x" labels indicate number of oxygen atoms in corresponding signals (excluding 3 oxygen atoms per nitrate functional group).

Table 1. Absorption cross section ($\sigma_{A,\lambda}$; cm^2) or A + B bimolecular rate constant (k_{A+B}, cm^3 $molec^{-1}$ s^{-1}) reference values.

σ or k	A	B	Value	Reference
$\sigma_{A,254}$	iPrONO	–	1.88×10^{-18}	1
$\sigma_{A,350}$	iPrONO	–	1.11×10^{-19}	1,2
$\sigma_{A,368}$	iPrONO	–	1.24×10^{-19}	1,2
$\sigma_{A,254}$	NO_2	–	1.05×10^{-20}	3
$\sigma_{A,350}$	NO_2	–	4.70×10^{-19}	3
$\sigma_{A,368}$	NO_2	–	5.60×10^{-19}	3
k	iPrONO	OH	7.20×10^{-13}	4
k	iPrONO-d_7	OH	2.73×10^{-13}	5
k	acetone	OH	1.94×10^{-13}	6
k	acetone-d_6	OH	3.21×10^{-14}	6
k	CH_3CHO	OH	1.5×10^{-11}	7
k	$CH_3C(O)O_2$	NO	9×10^{-12}	8
k	CH_3O_2	NO	7.7×10^{-11}	7
k	HCHO	OH	8.5×10^{-12}	7

[1]This work; [2]Raff and Finlayson-Pitts (2010); [3]Atkinson et al. (2004); [4]Raff and Finlayson-Pitts (2010); [5]Estimated from $k_{\mathrm{iPrONO+OH}}$ scaled by relative rate constants of n-C_3H_8 + OH and n-C_3D_8 + OH (Nielsen et al., 1988, 1991); [6]Raff et al. (2005); [7]Burkholder et al. (2015); [8]Orlando and Tyndall (2012).